

6. PLASMA TRANSIENT OPERATIONS

Farrokh Najmabadi
Robert A. Krakowski

Charles G. Bathke

Yuh-Yi Chu
Ronald L. Miller

Contents

6.1.	INTRODUCTION	6-1
6.2.	RFP START-UP DATA BASE	6-3
6.2.1.	Breakdown and Formation	6-4
6.2.2.	Current Ramp-Up	6-12
6.3.	FORMATION OF THE TITAN PLASMA	6-14
6.4.	IGNITION REQUIREMENTS	6-19
6.4.1.	Particle Balance	6-20
6.4.2.	Power Balance	6-21
6.4.3.	Energetic Alpha Particles	6-23
6.4.4.	Ignition Analysis	6-26
6.5.	CURRENT RAMP-UP TO IGNITION AND BURN	6-29
6.5.1.	Start-Up Sequence	6-29
6.5.2.	Circuit Model	6-34
6.5.3.	Plasma-Circuit Simulations	6-37
6.6.	SHUTDOWN & TERMINATION OF TITAN PLASMA	6-55
6.6.1.	Plasma Accidents	6-56
6.6.2.	Shutdown Procedures	6-57
6.6.3.	Termination Simulations	6-57
6.7.	SUMMARY AND CONCLUSIONS	6-62
	REFERENCES	6-65

6. PLASMA TRANSIENT OPERATIONS

6.1. INTRODUCTION

A typical reversed-field-pinch (RFP) experimental discharge can be divided into four phases: (1) breakdown and formation, (2) current ramp-up, (3) sustainment, and (4) termination. A representative time history of an RFP discharge, taken from ZT-40M experiments [1], is shown in Figure 6.1-1. Ignition and fusion burn in a reactor are achieved during the current ramp-up phase, and operation of the current-drive system is required during the sustainment phase. The breakdown and formation phase encompasses the time from the start, which begins by establishing a toroidal magnetic field inside the discharge chamber in the absence of the plasma, to the formation of a "seed" RFP plasma. At the time of peak toroidal magnetic field, poloidal-field windings are activated to produce a flux change through the center of the torus and, consequently, a toroidal voltage around the discharge chamber. This voltage typically ionizes the gas in a few microseconds and the toroidal current is initiated in the resulting plasma. The toroidal plasma current and the toroidal magnetic field within the plasma increase while the toroidal magnetic field at the wall decreases, keeping the average toroidal field (and the toroidal flux) in the chamber almost constant. Eventually the toroidal magnetic field at the wall changes sign and is crowbarred in the reverse direction relative to the back-biased condition of the breakdown and formation phase.

The plasma current is then increased to the peak value during the current ramp-up phase. The poloidal-field (PF) coil system provides the poloidal flux and the majority of toroidal flux contained within the full-current plasma by the RFP dynamo. The duration of an RFP experiment is extended by using either a passive crowbar applied to the poloidal circuits, to give a decaying waveform, or an active (power) crowbar to produce a flat-top current waveform. For a steady-state device, the sustainment phase requires operation of the current-drive system (oscillating-field current drive for TITAN).

Reversed-field-pinch discharges normally end abruptly and the plasma current decreases rapidly to zero. Accompanying this fast current "termination" is a positive pulse in the toroidal voltage at the liner, as is also shown on Figure 6.1-1. This current termination is in contrast to the negative spike in toroidal voltage that accompanies the current disruption in a tokamak, indicating a difference in the flow of magnetic energy to or from the plasma during the respective events. Furthermore, the RFP current termi-

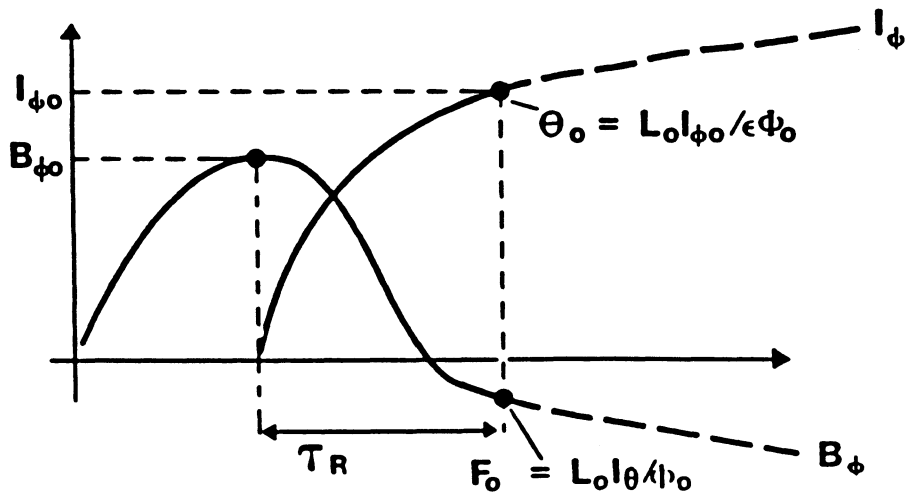
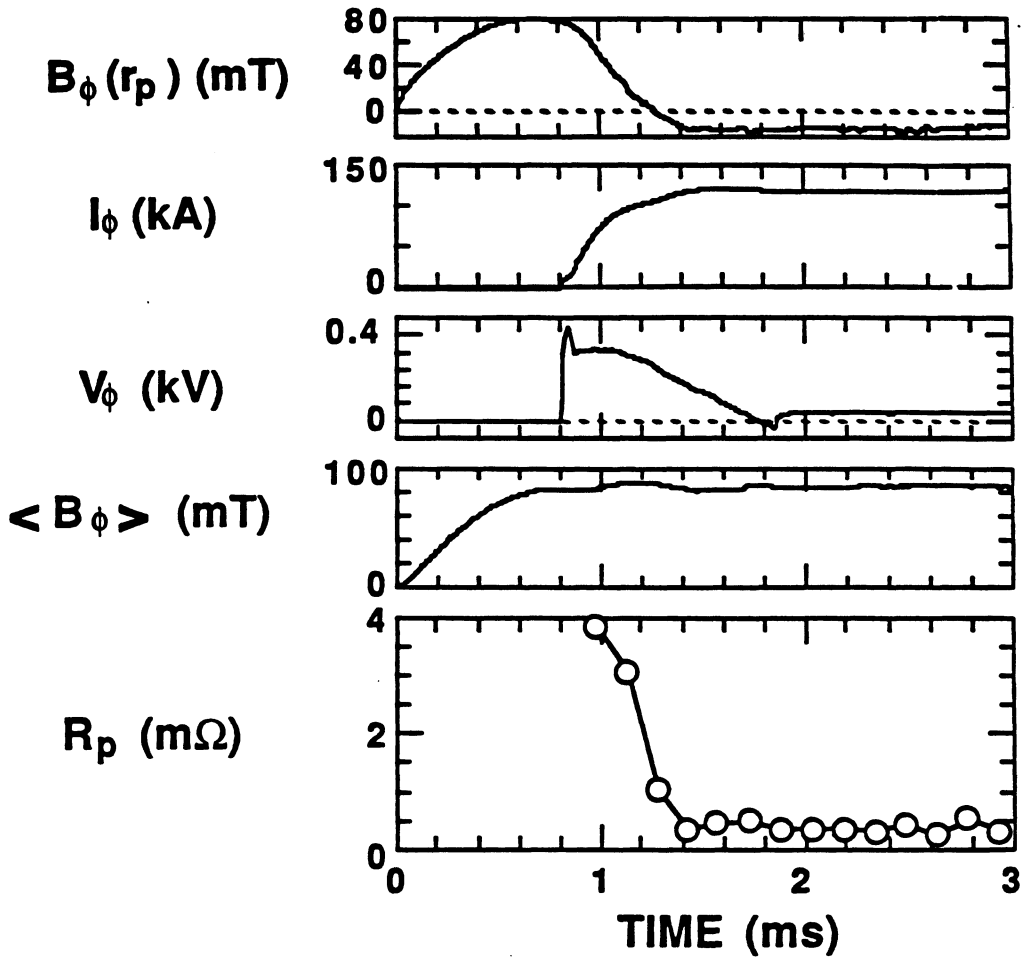


Figure 6.1-1. Typical matched-mode RFP formation for ZT-40M leading to the values of θ_0 , F_0 , and $I_{\phi 0}$ [1] used as initial conditions for start-up, ignition, and burn simulations.

nation can be influenced through the control of the density or toroidal magnetic field [2]; generally, the RFP terminates only when toroidal-field reversal is lost.

It became evident towards the end of the early RFP reactor studies [3] and during the scoping phase of the TITAN study [4] that the design limits for both the toroidal-field (TF) and PF coil systems would be determined more by the plasma breakdown, formation, and ramp-up transients than by the steady-state operational phase. The desire to use the RFP dynamo to generate internal toroidal flux (rather than injecting all the toroidal flux by the TF coils) and the constraints on bias stress and power strongly influence the TF and PF coil designs. Furthermore, the PF-coil configuration determines the coupling of ohmic-heating (OH) coils with the plasma, the magnitude of the stray vertical field, and the degree of multipolarity of field nulls in the plasma chamber. These in turn influence the breakdown and RFP formation conditions through the amount of initial (vacuum) toroidal field, B_{ϕ_0} , and ultimately affect the TF-coil design.

Section 6.2 reviews the existing RFP experimental data base for RFP formation and start-up, which is then applied to the TITAN designs (Section 6.3). The ignition requirements for ohmically heated RFPs are studied (Section 6.4) in order to identify the optimum path for TITAN start-up. Using the TITAN seed RFP conditions, a 0-D, profile-averaged plasma-circuit code is used to simulate the evolution of the TITAN plasma through current ramp, ignition, and burn transients (Section 6.5). Current termination is a safety and economic concern because of large magnetic stored energy in the TITAN plasma. Techniques for control of current termination and plasma shutdown, leading to a "soft-landing," are discussed in Section 6.6. Summary and conclusions are given in Section 6.7.

6.2. RFP START-UP DATA BASE

A body of experimental evidence is beginning to accumulate that better defines the windows for RFP breakdown, formation, and current ramp-up. The status in each of these areas is summarized. Although much of this information is not fully understood theoretically and extrapolation from ZT-40M-class experiments to a reactor is uncertain, nevertheless this information and experience is assimilated for the first time and used as part of the TITAN study [4].

Three modes of operation are generally used for RFP formation in present-day experiments: self-reversal, matched, and aided-reversal. In the self-reversal mode, a conducting shell maintains and conserves the toroidal flux inside the chamber. The self-reversal mode

of RFP formation is used on OHTE/RFP and often on HBTX1A. In the matched mode, the external circuits are programmed to conserve the toroidal flux inside the chamber by maintaining the poloidal electric field, E_θ , near zero at the liner, thereby simulating the action of a conducting shell. This mode is usually used on ZT-40M. In the aided-reversal mode, the external circuits supplement the plasma self-reversal effect, as is typically used on ETA-BETA-II. Field control during the formation phase provides flexibility in varying the pinch parameter, Θ , on which the configuration depends. The choice of the formation mode also affects the consumption of the poloidal flux during this phase of the RFP discharge. The final plasma parameters, however, are not particularly sensitive to the mode used for RFP formation.

In a conventional start-up sequence, the peak current is nearly reached at the time the toroidal field at the wall reverses (end of the formation phase). This start-up mode is undesirable in a large experiment or in a reactor because: (1) the RFP formation phase is power intensive until reversal is reached, and (2) large voltages are required. It is advantageous to set up the RFP configuration in a relatively short time at a low current and low stored energy and then slowly increase the current to the desired value while maintaining the RFP profiles. This mode of RFP start-up, called the ramped start-up, has been demonstrated on the ZT-40M experiment. Figure 6.1-1 shows such a ramped start-up, as well as the formation phase and key notation.

The ramped start-up scenario relies on the plasma relaxation process. During the current ramp, the toroidal flux must be increased proportionally to the current to maintain the RFP profiles while holding F and Θ constant. This process requires the generation of toroidal flux by the RFP dynamo, since the toroidal field at the wall is negative while the average toroidal flux within the conducting shell is positive. The plasma must generate an equal and opposite amount of negative and positive flux to satisfy Faraday's law and then expel the negative flux from the plasma to generate a net positive flux increase. Indeed, the ramped discharges show that toroidal flux (Figure 6.1-1) continues to be generated, and negative flux is expelled from the plasma; this process occurs on a multi-millisecond time scale. Ramped start-up operation has also recently been reported for the HBTX1B experiment [5]. The TITAN reactor design also relies on a rapid formation of a "seed" RFP followed by a slow plasma-current ramp to the final value.

6.2.1. Breakdown and Formation

Plasma discharge and subsequent RFP formation generally occurs for values of the ratio of toroidal electric field to initial filling pressure, E_ϕ/P_o , that are similar to tokamak

values, but closer to electron runaway conditions. For example, for the JET experiment, a value of $E_\phi/P_o \geq 0.66 \times 10^4$ V/m-torr is reported [6], compared to 1 to 2×10^4 V/m-torr for ZT-40M [7], which is close to electron runaway conditions. Figure 6.2-1 gives typical breakdown and formation characteristics for a range of tokamaks [8] and for ZT-40M [9, 10]. Generally, breakdown and discharge formation are not problems for RFPs, but the degree of pre-ionization can greatly influence the discharge quality and poloidal-flux consumption [9,10]. Since, to date, stable and reliable RFP formation appears to require a high E_ϕ , the generally common E_ϕ/P_o values for both RFPs and tokamaks give significantly higher values of P_o required to create a robust RFP. An initial electric field of $E_\phi = 55$ V/m is indicated in Figure 6.1-1 for matched-mode operation.

A toroidal-field line of strength, $B_{\phi o}$, in the presence of a vertical field, B_V , will intersect the first wall and thereby prevent the formation of a continuous discharge if the ratio $B_V/B_{\phi o}$ is too large. The condition for the confinement of a single toroidal trajectory with a field null at a minor radial position, r_o , is given by

$$\frac{B_V}{B_{\phi o}} \leq \frac{\epsilon}{2\pi} \sqrt{1 - (r_o/r_p)^2}, \quad (6.2-1)$$

where $\epsilon = r_p/R_T$ is the inverse plasma aspect ratio. For TITAN with $1/\epsilon \simeq 6.5$ and setting $r_o \simeq r_p/4$, Equation 6.2-1 results in $B_V/B_{\phi o} \lesssim 0.02$.

In addition, a drift constraint, $E_\phi/(B_V/B_{\phi o}) \geq 10^3$ V/m, has been suggested for JET [8]. This drift constraint together with Equation 6.2-1 results in $E_\phi \geq 22$ V/m, which is about a factor of 2 below experimental values derived from the ZT-40M experience. Therefore, breakdown voltage in the range 500 to 1,000 V may be required for the reactor. Careful designs that minimize field errors can possibly reduce these start-up voltages.

Therefore, in characterizing the TITAN initial conditions, the following possible constraints on the toroidal electric field were considered:

$$\left\{ \begin{array}{ll} \frac{E_\phi}{P_o} \geq 6.6 \times 10^3 \text{ V/m-torr} & \text{JET breakdown} \\ \frac{E_\phi}{B_V/B_{\phi o}} \geq 10^3 \text{ V/m} & \text{JET drift} \\ \frac{E_\phi}{P_o} \simeq 1 - 2 \times 10^4 \text{ V/m-torr} & \text{ZT-40M} \end{array} \right. \quad (6.2-2)$$

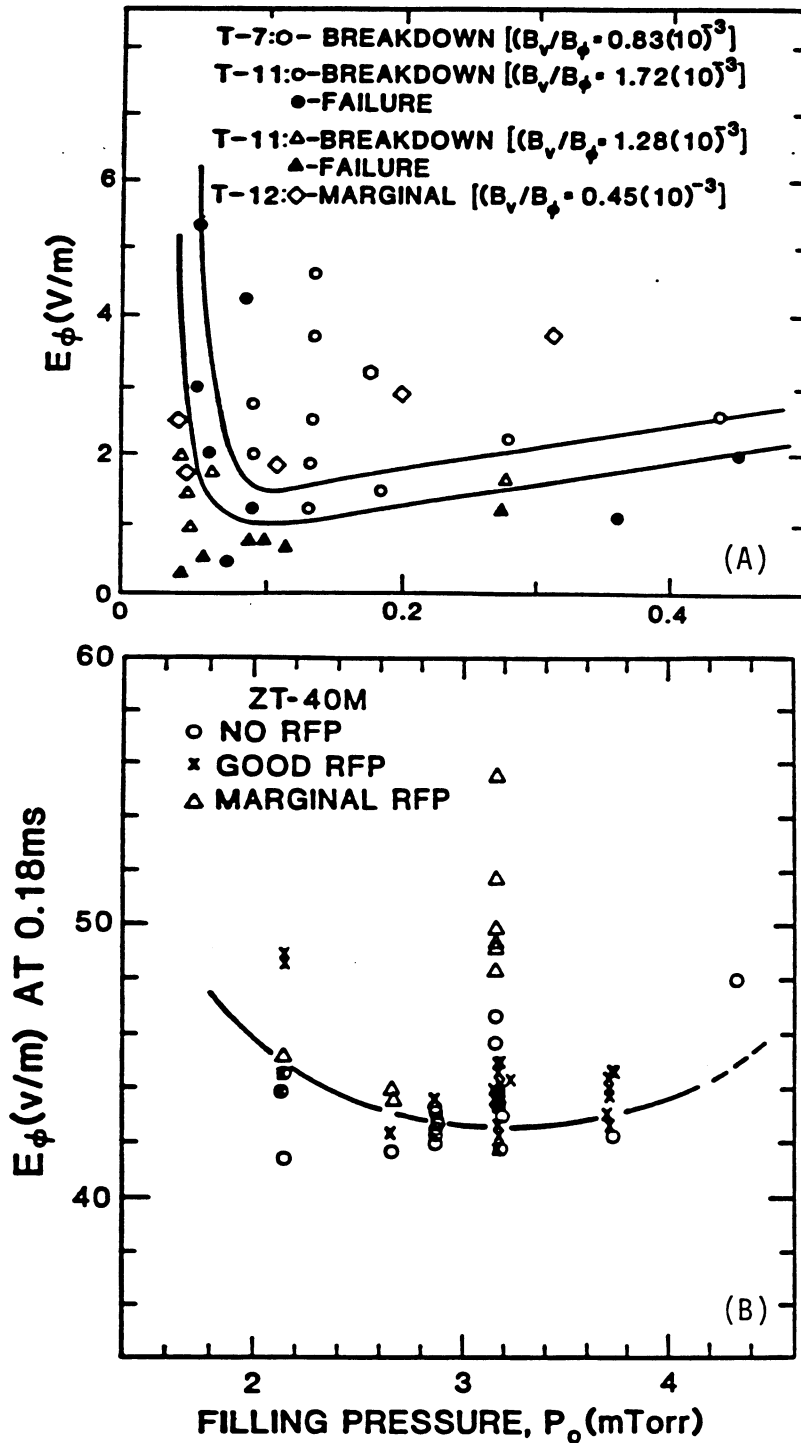


Figure 6.2-1. Typical breakdown curves for (A) tokamak [8] and (B) RFP formation [9, 10].

In order to establish the parameters of the seed RFP, the relationship between $B_{\phi o}$ and the average toroidal flux within the initial RFP, $\langle B_{\phi} \rangle$, must be determined (Figure 6.1-1). Generally, $\langle B_{\phi} \rangle \simeq B_{\phi o}$ for RFP formation. Figure 6.2-2 shows the relationship between $B_{\phi o}$ and $\langle B_{\phi} \rangle$ for a range of ZT-40M discharges, illustrating the experimental basis for this assumption. For a given $\langle B_{\phi} \rangle$ and the initial pinch parameter, Θ_o , the initial (minimum) RFP current or current density is determined from

$$I_{\phi o} = 5 \times 10^6 r_p \Theta_o \langle B_{\phi} \rangle. \quad (6.2-3)$$

Hence, for $\langle B_{\phi} \rangle \simeq B_{\phi o} = 0.05$ T at formation, and TITAN plasma conditions of $\Theta_o \simeq 1.5$ and $r_p = 0.6$ m, the initial RFP current is $I_{\phi o} \simeq 0.2$ MA.

Although the specification of Θ_o and $\langle B_{\phi} \rangle$ at formation determines an initial current density (e.g., $j_{\phi o} \simeq 0.2$ MA/m² for above example for TITAN), other more dominant constraints may exist. For example, the ZT-40M experiment exhibits a minimum current-density limit which translates empirically to $j_{\phi o} \geq 0.4$ MA/m², below which RFP formation is difficult. This constraint is not well understood, but the application of such a constraint to TITAN represents a conservative connection to experiment and for the above condition would require a doubling of $B_{\phi o} \simeq \langle B_{\phi} \rangle$. Secondly, a number of RFP experiments [11] have shown an impurity burn-through constraint, shown in Figure 6.2-3 for ZT-40M. For these conditions, burn-through requires that

$$\frac{j_{\phi}}{n} \geq 10^{-14} \text{ A m}. \quad (6.2-4)$$

This constraint, however, when applied to the 0.2- to 0.4-keV plasmas expected for these formation conditions may place the plasma strongly in the electron runaway regime. If the runaway regime is to be avoided, which may or may not be a requirement, higher densities will be required (e.g., for $\xi \equiv v_D/v_{THe} \sim 0.01$, $n \geq 2 \times 10^{19}$ m⁻³ for $j_{\phi} = 0.4$ MA/m² and $T \simeq 0.2$ keV).

Generally, if the density pump-out is too great prior to toroidal-field reversal for a given initial filling pressure, P_o , unreliable RFP formation occurs [7], as is shown in Figure 6.2-4(A). Similarly, for a given P_o , a maximum initial bias field, $B_{\phi o}$, is found above which RFP formation does not occur [7], as is shown in Figure 6.2-4(B). Although RFPs form at lower values of $B_{\phi o}$, these RFPs have excessive poloidal-flux consumption, as is also shown in Figure 6.2-4(B), for the ZT-40M conditions examined. It should be noted that a variable and poorly controlled wall condition creates hystereses and related unpredictable effects in many of these data correlations. The constraints of Figures 6.2-4(A) and (B) have been combined in Figure 6.2-4(C) to eliminate the filling

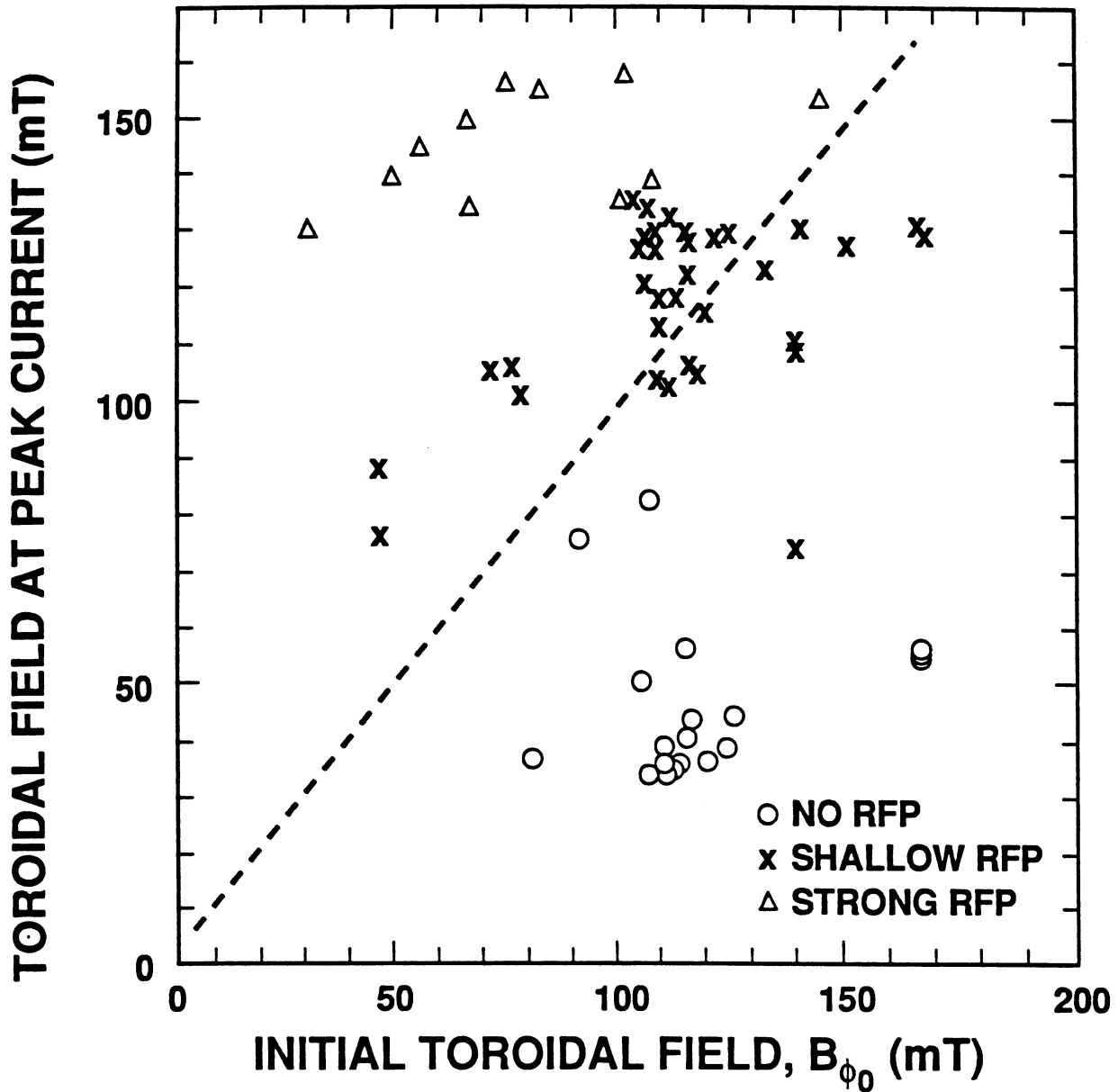


Figure 6.2-2. Relationship between B_{ϕ_0} and $\langle B_{\phi} \rangle$ for a range of ZT-40M discharges [7, 10] where robust RFP formation occurred, as well as no RFP formation and/or very shallow, spheromak-like RFPs were formed.

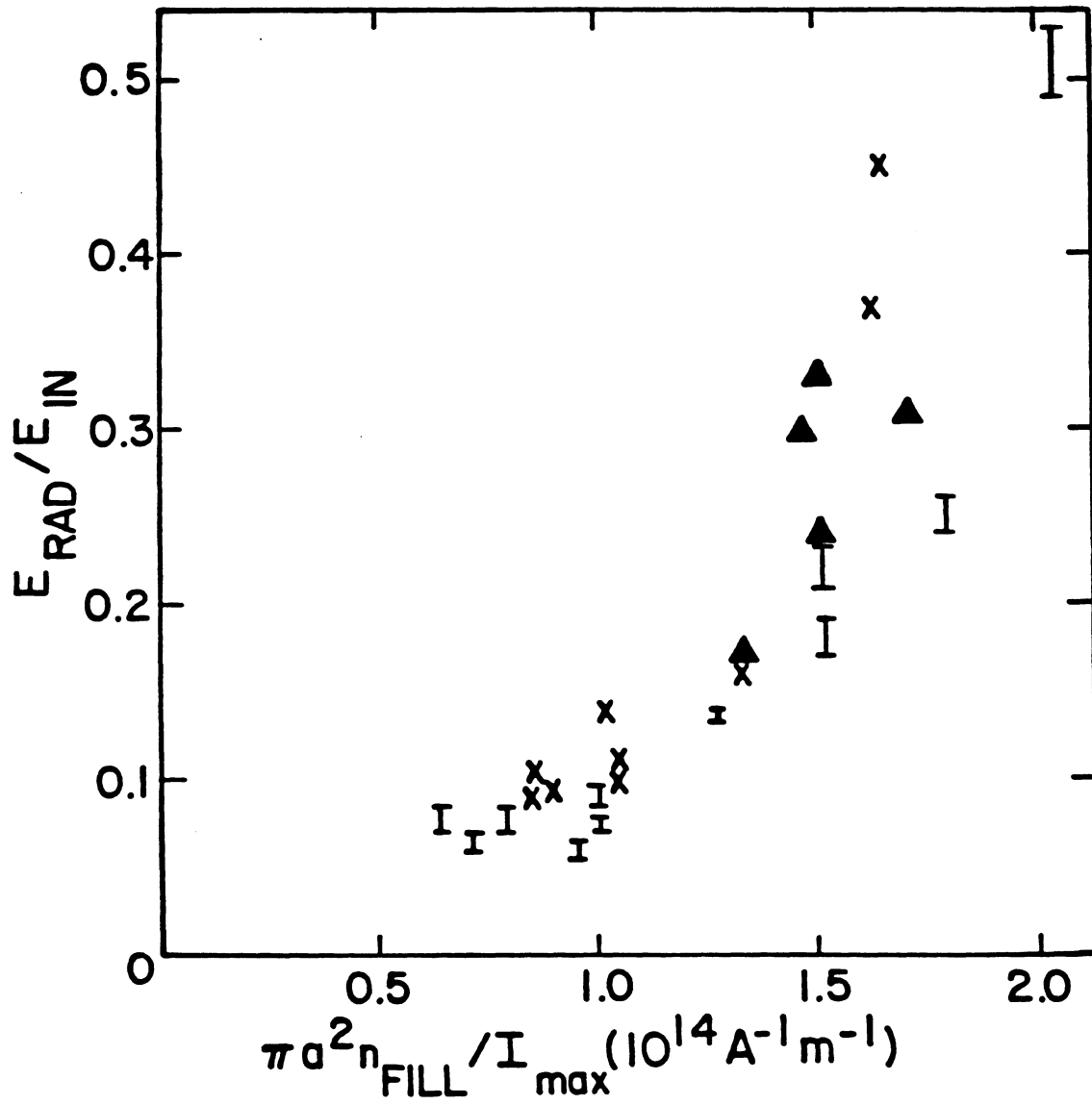


Figure 6.2-3. Typical impurity burn-through constraint for ZT-40M [7].

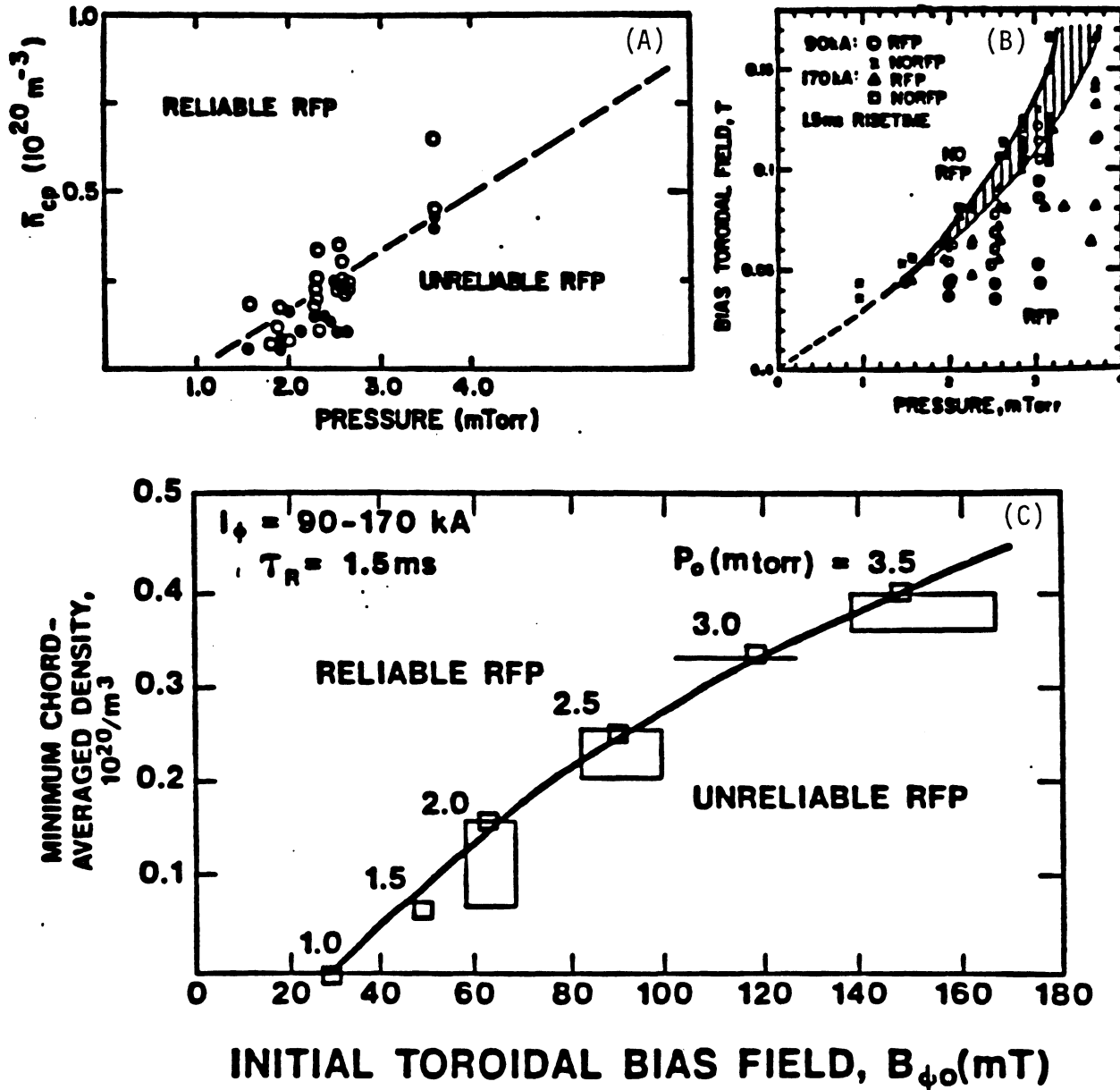


Figure 6.2-4. Typical RFP formation windows showing: (A) dependence on a critical plasma density, (B) magnitude of the initial toroidal bias field, and (C) a combination of the two constraints [7].

pressure as a variable and perhaps to reduce the impact of these unresolved wall effects on these data. The result is a relationship between minimum plasma density and initial bias field that may be useful in assuring robust RFP formation:

$$n \geq \begin{cases} 10^{19} & \text{for } B_{\phi_0} < 0.036 \text{ T} \\ 2.78 \times 10^{20} B_{\phi_0} & \text{for } B_{\phi_0} > 0.036 \text{ T} \end{cases} \quad (6.2-5)$$

Most present-day RFPs experience a significant loss of density or pump-out upon formation, as is shown in Figure 6.2-5. The degree of density reduction between the initial filling pressure and the final RFP formation is not well understood but it depends strongly on wall preconditioning. Hence, the pump-out is expressed in terms of the ratio of initial filling density, n_o , to the final RFP plasma density, n , and the assumption must be made for the reactor that pump-out and P_o can be minimized, thereby minimizing the E_ϕ required under start-up conditions.

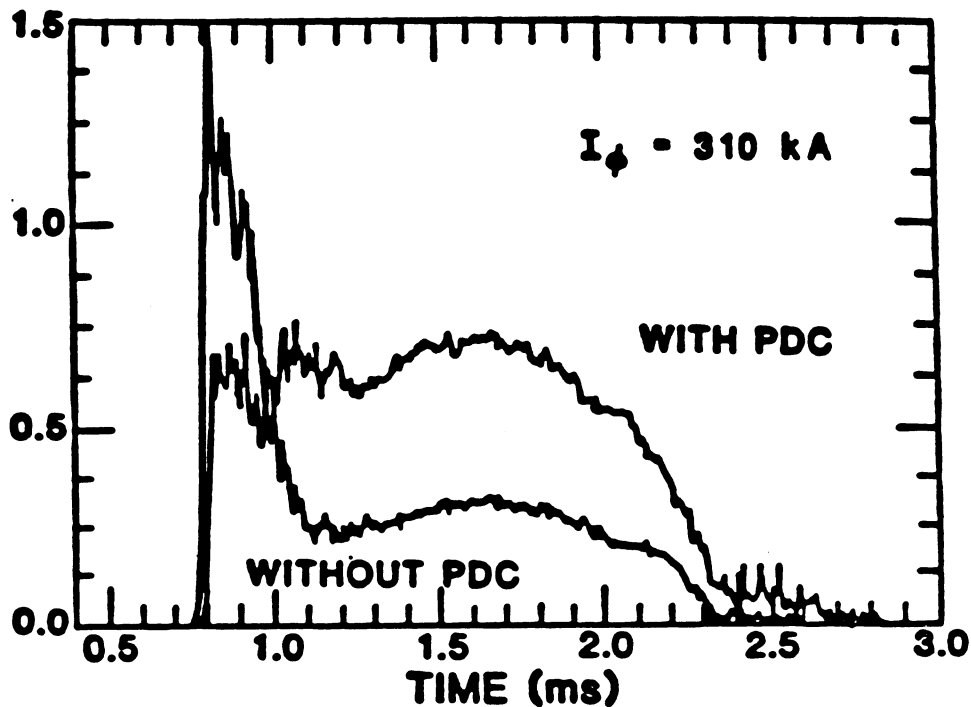


Figure 6.2-5. Loss of density or pump-out for a typical ZT-40M discharge. Also shown is the impact of pellet fueling on reducing pump-out [12].

6.2.2. Current Ramp-Up

While the formation phase leading to the low-current (~ 0.2 -MA) seed RFP is characterized by a rapid current rise (150 MA/s for the case shown in Figure 6.1-1), and the flux consumption can be a small fraction of the inductive flux delivered to the plasma, the subsequent current ramp to ohmic ignition and burn in the TITAN plasma ($I_\phi = 18$ MA) represents a greater concern from the viewpoint of resistive flux consumption and the implication on OH-coil and related power-supply designs.

Figure 6.2-6 shows that slow current ramp rates (9 MA/s) have been achieved in ZT-40M. These current ramp rates are still large compared to those typical of tokamaks (1 to 2 MA/s) and are possible in RFPs because of the anomalous penetration of magnetic flux. The slow current ramps of the kind shown are desirable for reactors since the bulk of the flux injection can be supplied directly from the electrical grid at relatively low power, rather than from an expensive on-site energy storage.

A significant decrease in plasma loop voltage is measured upon reversal of the toroidal field and formation of the RFP. This behavior is shown for ZT-40M in Figure 6.2-7, which also shows an optimal value of the pinch parameter from the viewpoint of loop voltage and

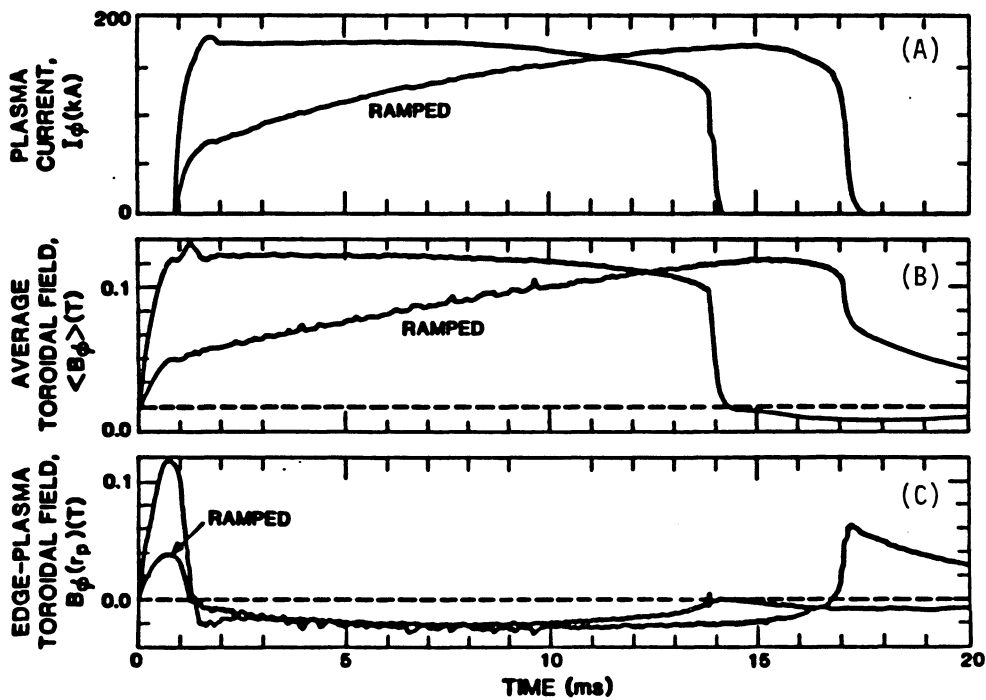


Figure 6.2-6. Slow and fast current ramps in ZT-40M [7].

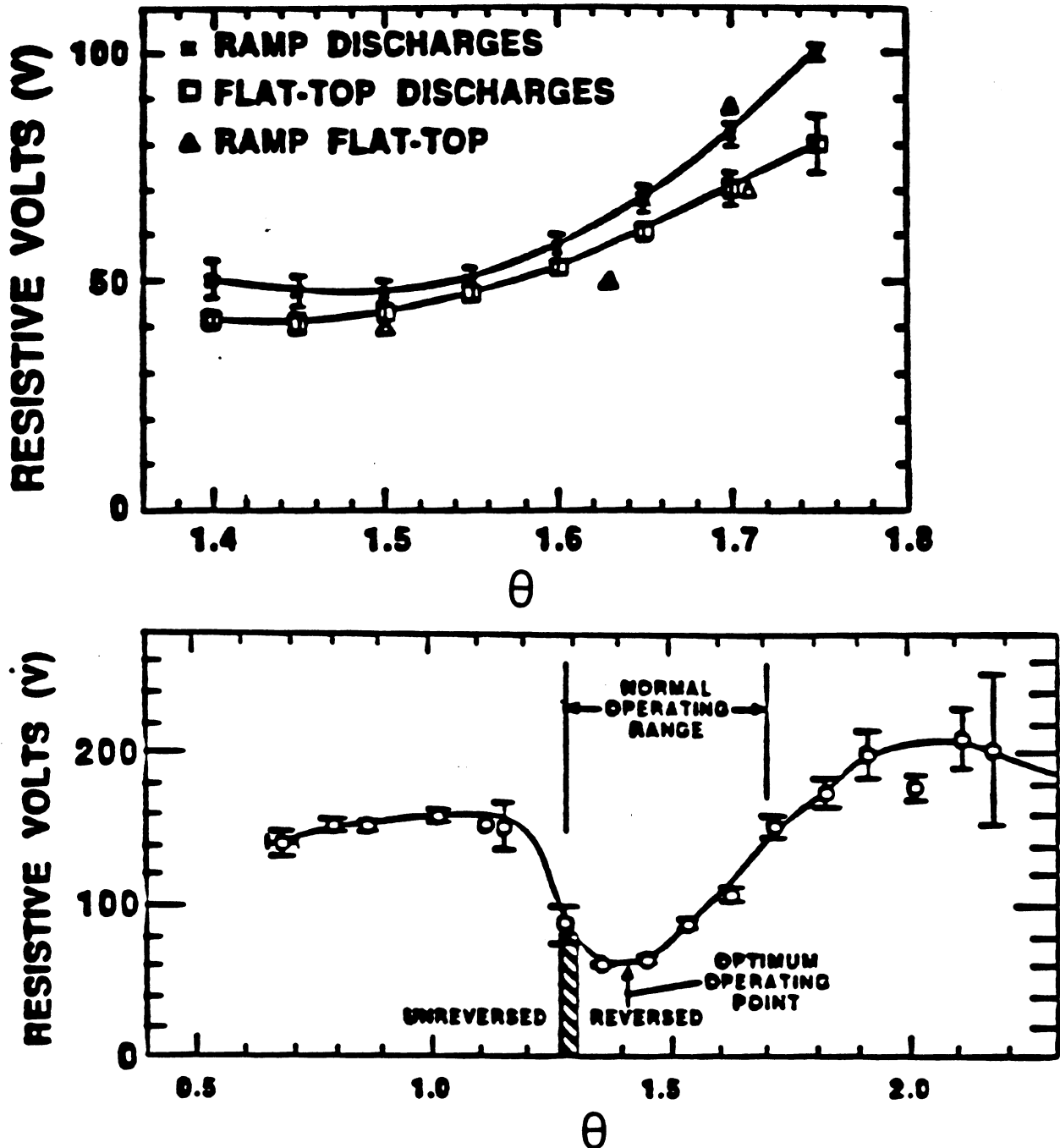


Figure 6.2-7. The dependence of the plasma loop voltage on the pinch parameter upon formation of RFP, showing an optimal value of θ [1].

resistive poloidal-flux consumption. The reduction in resistive flux consumption upon controlling Θ at the optimal value is shown in Figure 6.2-8, which gives the resistive volt-second consumption for a range of conditions, including the volt-second efficient matched-mode operation. The ZT-40M data shown on Figure 6.2-8 indicate a constant (resistive) voltage scaling ($V_{RES} \simeq 32.5$ V), which implies that the plasma resistance is decreasing inversely with plasma current in this region. The implication of this scaling on the TITAN-I reactor design is examined in Section 8.5.3.

6.3. FORMATION OF THE TITAN PLASMA

In this section, the set of constraints and options for breakdown and RFP formation described in Section 6.2 are applied to the TITAN plasma formation. The notation used here follows that of the previous section in that a o subscript denotes the parameters of the seed RFP with the exceptions of $B_{\phi o}$, n_o , and P_o which denote, respectively, the initial (bias) toroidal field, and the fill gas density and pressure. It is further assumed that

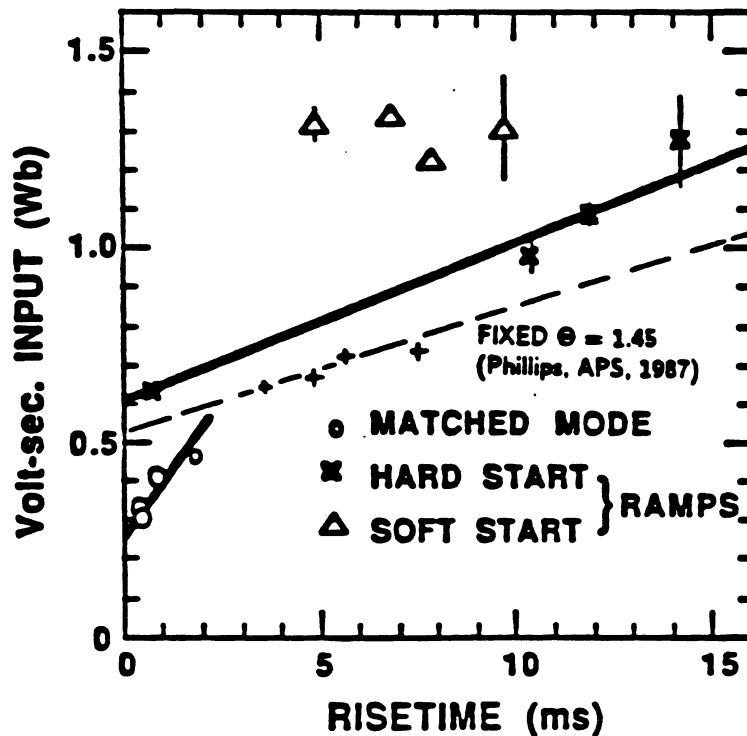


Figure 6.2-8. Dependence of flux input on current risetime for a range of ZT-40M operating conditions [1,7].

during the RFP formation phase, the toroidal flux inside the plasma chamber remains constant (*i.e.*, $\langle B_\phi \rangle = B_{\phi o}$) and the density pump-out is minimized (*i.e.*, $n = n_o$).

Vertical-field constraint. Applying Equation 6.2-1 to the TITAN designs with $1/\epsilon = 6.5$ and $r_o \leq r_p/4$ results in $B_V/B_{\phi o} \leq 0.024$. The stray vertical field for TITAN-I and TITAN-II designs are, respectively, 0.43 and 2.3 mT (Section 4.5). Therefore, minimum initial bias fields are $B_{\phi o} \geq 18$ mT for TITAN-I and $B_{\phi o} \geq 97$ mT for TITAN-II.

Density and current-density constraints. The impurity burn-through constraint, Equation 6.2-4, results in a minimum value for j_ϕ/n . Assuming that $B_{\phi o} > 0.036$ T in Equation 6.2-5 and substituting for $\langle B_\phi \rangle = B_{\phi o}$ from Equation 6.2-3 results in a maximum value for j_ϕ/n . For TITAN plasma conditions of $\Theta_o \simeq 1.5$ and $r_p = 0.6$ m, then

$$10^{-14} < \frac{j_\phi}{n} \text{ (A m)} < 1.43 \times 10^{-14}. \quad (6.3-1)$$

Although the specification of Θ_o and $\langle B_\phi \rangle$ at formation determines an initial current density, other more dominant constraints may exist. First, the ZT-40M experiment exhibits a minimum current-density limit, which translates empirically to $j_{\phi o} \geq 0.4$ MA/m², below which RFP formation is difficult. This constraint is not well understood, but its application to TITAN represents a conservative connection to experiment. Second, the maximum value of the poloidal beta of the seed RFP, $\beta_{\theta o}$, results in another constraint on the minimum value of j_ϕ and/or the maximum value of n . The temperature of the seed RFP should also be reasonable for the chosen value of j_ϕ . Third, high values of current density (and/or low n) may place the plasma strongly in the electron runaway regime. If the runaway regime is to be avoided, which may or not may be a requirement, the electron drift parameter should be limited to $\xi \lesssim 0.01$, where

$$\xi = \frac{v_D}{v_{THe}} = \frac{1.05 \times 10^{13}}{\sqrt{T_e}} \frac{j_\phi}{n}, \quad (6.3-2)$$

and SI units are used except for temperature which is in eV.

Based on the above discussion, the current density in the reference seed TITAN plasma is set at $j_{\phi o} = 0.4$ MA/m² in order to provide a conservative connection to the ZT-40M experiment. This choice results in $I_{\phi o} = 0.45$ MA and $B_{\phi o} = \langle B_\phi \rangle = 100$ mT which satisfies the stray vertical-field constraint for both TITAN-I and TITAN-II designs. The temperature and density of the seed plasma are set, respectively, at $T_e = 100$ eV and

$n_o \simeq n = 2.8 \times 10^{19} \text{ m}^{-3}$. The corresponding gas (D_2) fill pressure is $P_o = 0.4 \text{ mtorr}$. This value of n is the minimum density that satisfies Equation 6.3-1 and it is chosen to ensure $\beta_{\theta o} = 0.1$. The resulting drift parameter, however, is $\xi = 0.015$.

The above set of parameters for the TITAN seed RFP is not unique and reflects a compromise among breakdown and formation constraints. For example, higher plasma temperatures can be obtained for higher values of $\beta_{\theta o}$, which also reduce the value of ξ ($T_e = 200 \text{ eV}$ and $\xi = 0.011$ for $\beta_{\theta o} = 0.2$). Alternatively, one can increase n to $4 \times 10^{19} \text{ m}^{-3}$ (corresponding to $j_\phi/n = 10^{-14} \text{ A m}$) to have $\xi = 0.011$ and $\beta_{\theta o} = 0.14$ for $T_e = 100 \text{ eV}$. Finally, in order to reduce formation energy and flux consumption, $j_{\phi o}$ can be reduced to 0.28 MA/m^2 , relaxing the $j_{\phi o} = 0.4 \text{ MA/m}^2$ connection to ZT-40M. Then, choosing $n_o \simeq n = 2.8 \times 10^{19} \text{ m}^{-3}$ ($j_\phi/n = 10^{-14} \text{ A m}$) results in $\xi = 0.011$ and $\beta_{\theta o} = 0.2$ for $T_e = 100 \text{ eV}$. For this case, however, the initial bias field is $B_{\phi o} = \langle B_\phi \rangle = 70 \text{ mT}$, which satisfies the stray vertical-field constraint for TITAN-I but violates this constraint for TITAN-II.

Toroidal electric-field constraint. Given the reference parameters of the TITAN seed RFP, the necessary toroidal electric field can be found from Equation 6.2-2 to be $E_{\phi o} \gtrsim 2.6 \text{ V/m}$ from the JET breakdown condition and $E_{\phi o} \gtrsim 4$ to 8 V/m from the ZT-40M constraint. Note that the $E_{\phi o}$ value from the ZT-40M constraint is an order of magnitude lower than that actually used in the ZT-40M experiment ($\sim 40 \text{ V/m}$) because the gas fill pressure in TITAN is much lower. The JET drift condition results in $E_{\phi o} \gtrsim 4.3 \text{ V/m}$ for TITAN-I and $E_{\phi o} \gtrsim 23 \text{ V/m}$ for TITAN-II. This wide range of $E_{\phi o}$ translates into a loop voltage, $V_\phi \equiv 2\pi R_T E_\phi$, in the range of 100 to 500 V.

Low values of loop voltage are desirable because they reduce the requirements on the power supplies and the insulation of the vessel. On the other hand, higher loop voltages reduce the RFP formation time and may result in reducing the necessary resistive energy and volt-seconds. In order to estimate the resistive energy consumed during the formation phase, we ignore the compressional and resistive voltages during the initial phase of the RFP formation, and approximate the current rise time by a sinusoidal, inductive waveform (capacitor power supply). The current rise time, τ_R , is then:

$$\frac{I_{\phi o}}{\tau_R} = \frac{2}{\pi} \frac{V_{\phi o}}{L_p}, \quad (6.3-3)$$

where L_p is the plasma internal inductance ($L_p = 13.3 \mu\text{H}$ for the TITAN plasma). For the ZT-40M experiment, $I_{\phi o}/\tau_R \sim 30$ to 40 MA/s while for TITAN, $I_{\phi o}/\tau_R \sim 4.5$ to 22 MA/s (for $E_{\phi o} \sim 4$ to 20 V/m).

Poloidal flux consumption. In addition to the required inductive flux, $L_p I_{\phi o}$, the resistive flux consumption during the breakdown and formation phase can be estimated using the average resistivity of

$$\eta = 4.91 \times 10^{-2} I_{\phi o}^{-0.64}, \quad (6.3-4)$$

which has been reported for the matched-mode start-up of the ZT-40M experiment [1]. It can be assumed that the above relationship can be directly applied to the TITAN plasma. Alternatively, one can assume that plasmas with similar current densities have similar resistivities. In the latter case, the resistivity of the TITAN plasma during formation is

$$\eta = 3.85 \times 10^{-1} r_p^{1.28} I_{\phi o}^{-0.64}, \quad (6.3-5)$$

which indicates a fivefold increase in the TITAN plasma resistance compared with estimates from Equation 6.3-4.

Assuming that the resistivity remains constant during the formation phase, the resistive portion of the formation energy is

$$\begin{aligned} W_{RES} &= (2\pi R_T)(\pi r_p^2) \int_0^{\tau_R} \eta j_\phi^2 dt \\ &= \frac{R_T}{r_p^2} \eta I_{\phi o}^2 \tau_R, \end{aligned} \quad (6.3-6)$$

and the resistive flux consumption is

$$\int_0^{\tau_R} V_\phi dt = \frac{2}{I_{\phi o}} W_{RES}. \quad (6.3-7)$$

The parameters of the TITAN seed RFP are given in Table 6.3-I. The formation time, energy, and flux consumption are calculated for both estimates of the TITAN plasma resistivity (Equations 6.3-4 and 6.3-5). The formation parameters are reported for three values of toroidal electric field of 4, 8, and 20 V/m to cover the range of required loop voltages discussed previously and also to study the resultant resistive flux consumption. Table 6.3-I shows that as $E_{\phi o}$ is increased from 4 to 20 V/m, the formation time is reduced from 100 to 20 ms and the resistive flux consumption and formation energy decrease by fivefold. For $E_{\phi o} = 20$ V/m and plasma resistivity scaling with current (Equation 6.3-3), the resistive components of flux consumption and formation energy become small compared to the total values, while for $E_{\phi o} = 4$ V/m, the resistive components dominate.

In summary, the conditions for plasma breakdown and subsequent RFP formation for the reactor are expected to differ little from the conditions in present and planned

Table 6.3-I.

PARAMETERS OF RFP FORMATION PHASE FOR TITAN

Plasma current, I_{ϕ_0} (MA)		0.452	
Plasma current density, j_{ϕ_0} (MA/m ²)		0.400	
Initial toroidal field, B_{ϕ_0} (T)		0.100	
Average toroidal field, $\langle B_{\phi} \rangle$ (T)		0.100	
Toroidal field at r_p , $B_{\phi}(r_p)$ (T)		-0.010	
Poloidal field at r_p , $B_{\theta_0}(r_p)$ (T)		0.151	
Pinch parameter, Θ_0		1.5	
Reversal parameter, F_0		-0.1	
Poloidal beta, β_{θ_0}		0.1	
Drift parameter, ξ		0.015	
Fill pressure, P_0 (mtorr)		0.395	
Plasma density, n (m ⁻³)		2.80×10^{19}	
Electron temperature, T_e (keV)		0.100	
Toroidal electric field, E_{ϕ_0} (V/m)	4.0	8.0	20.
Loop voltage V_{ϕ_0} (V)	98.0	196.	490.
Formation time, τ_R (ms)	101.	50.4	20.2
Resistivity from Equation 6.3-3			
Resistive flux consumption (Wb)	11.7	5.8	2.33
Total flux consumption (Wb) ^(a)	17.9	12.1	8.62
Resistive formation energy (MJ)	2.64	1.32	0.53
Total formation energy (MJ) ^(a)	4.06	2.74	1.95
Resistivity from Equation 6.3-4			
Resistive flux consumption (Wb)	47.5	23.8	9.5
Total flux consumption (Wb) ^(a)	53.8	30.0	15.8
Resistive formation energy (MJ)	10.8	5.38	2.15
Total formation energy (MJ) ^(a)	12.2	6.80	3.57

(a) Including $L_p I_p = 6.29$ Wb and $0.5 L_p I_p^2 = 1.42$ MJ.

RFP experiments [13]. Likewise, the conditions of the seed RFP plasma required to start up the TITAN reactor, except for plasma size, are similar to present-day RFP parameters ($I_\phi = 0.2$ to 0.4 MA, $n = 1$ to $3 \times 10^{19} \text{ m}^{-3}$, $T = 0.1$ to 0.4 eV). For the reference formation scenario, loop voltage in the range of 200 to 500 V is necessary to ensure short formation time and acceptable resistive flux consumption and formation energy. The scaling of plasma resistivity during the formation phase is an important issue that may be resolved with data from larger RFP experiments. Better density and impurity control during the breakdown and formation process may also be required.

Formation of a seed RFP with somewhat smaller $j_{\phi o}$ (and lower $B_{\phi o}$ and n but higher $\beta_{\theta o}$) would reduce the formation time and is desirable (but requires the relaxation of $j_{\phi o} = 0.4 \text{ MA/m}^2$ connection to ZT-40M). For example, $j_{\phi o} = 0.28 \text{ MA/m}^2$ and $n_o \simeq n = 2.8 \times 10^{19} \text{ m}^{-3}$ ($j_\phi/n = 10^{-14} \text{ A m}$) result in $\xi = 0.011$ and $\beta_{\theta o} = 0.2$ for $T_e = 100 \text{ eV}$. This 30% reduction in $j_{\phi o}$ results in 30% reduction in τ_R , 40% reduction in resistive flux consumption, and 60% in resistive formation energy for the same value of $E_{\phi o}$. For this case, however, the initial bias field is $B_{\phi o} = \langle B_\phi \rangle = 70 \text{ mT}$, which satisfies the stray vertical-field constraint for TITAN-I but violates this constraint for TITAN-II.

6.4. IGNITION REQUIREMENTS

The steady-state analysis of global plasma power balance provides useful information for the optimization of the plasma approach to ignition. Results of this type of analysis for auxiliary-heated fusion devices are usually presented in the form of required auxiliary power for power balance as a function of plasma density and temperature. This information is then used to identify the path to ignition that requires minimum auxiliary heating power. Similar analysis can be applied to compact RFP reactors in which the plasma is heated to ignition by ohmic heating alone (no auxiliary heating).

The plasma models used for this analyses are reported in this section and they are also used for the plasma-circuit interaction code of Section 6.5. The plasma parameters reported throughout this section are all volume-averaged quantities, that is

$$n \equiv \frac{2}{r_p^2} \int_0^{r_p} n(r) r dr, \quad (6.4-1)$$

except as otherwise noted. For example, the temperature is defined as:

$$T \equiv \frac{2}{n r_p^2} \int_0^{r_p} n(r) T(r) r dr, \quad (6.4-2)$$

which is density-weighted volume averaged so that the plasma pressure represents a volume-averaged quantity.

The plasma profiles used in the transient analyses are based on the equilibrium analyses of Section 5.2. For the TITAN plasma analysis, two distinct sets of μ and p profiles have been used. For start-up and transient calculations of this section, a standard set of profiles,

$$\mu(r) = \mu(0) \left[1 - (r/r_p)^8 \right], \quad (6.4-3)$$

$$n(r) = n(0) \left[1 - (r/r_p)^{2.5} \right], \quad (6.4-4)$$

$$T(r) = T(0) \left[1 - (r/r_p)^4 \right], \quad (6.4-5)$$

are used. At steady-state full-power operation, the TITAN plasma is deliberately doped with a trace amount of Xe impurity to enhance core-plasma radiation and to reduce the heat load on the divertor target plates. One-dimensional transport analysis (Section 5.3) has been performed and the following plasma profiles were obtained:

$$\mu(r) = 2.843 \left[1 - 0.44 (r/r_p)^6 - 0.56 (r/r_p)^8 \right], \quad (6.4-6)$$

$$T_e(r) = \begin{cases} 14.40 - 46.94 (r/r_p)^{2.8504} & (0 < r/r_p < 0.25) \\ 16.07 - 10.29 (r/r_p) & (0.25 < r/r_p < 0.833) \\ 8.111 - 7.886 (r/r_p)^{14.025} & (0.833 < r/r_p < 1) \end{cases}, \quad (6.4-7)$$

$$n(r) = 1.23 \times 10^{21} \left[1 - 0.8577 (r/r_p)^{3.44} \right]. \quad (6.4-8)$$

These profiles have been used in the simulation of the steady-state, burning plasma of TITAN designs. The normalized profiles of plasma parameters (n , T , P , and μ), magnetic field, current density, and safety factor, q , for both sets of profiles are shown in Figures 5.2-1 through 5.2-4.

6.4.1. Particle Balance

The particle balance equation for ion species "j" ($j = D, T, {}^4\text{He}, \text{etc.}$) is

$$\frac{dn_j}{dt} = S_j - \frac{n_j}{\tau_{pj}} - R_j. \quad (6.4-9)$$

Here S_j is the particle source strength, τ_{pj} is the effective particle confinement of species "j" (including recycling), and R_j is the loss rate of particle due to fusion reactions (if

they fuse). The electron density is obtained from charge neutrality condition,

$$n_e = \sum_j Z_j n_j, \quad (6.4-10)$$

where Z_j is the atomic number of ion species "j". The effective plasma charge, Z_{eff} is given by,

$$Z_{eff} = \frac{1}{n_e} \sum_j n_j Z_j^2. \quad (6.4-11)$$

In the study of TITAN start-up, ignition requirement analyses of Section 6.4.4 are used to find an "optimum" density evolution, $n(t)$, which results in the shortest and most effective approach to ignition. Equation 6.4-9 is then used to compute the corresponding fueling rate, S_j .

6.4.2. Power Balance

The power balance equation for ion species "j" ($j = D, T, {}^4\text{He}, \text{etc.}$) is

$$\frac{3}{2} \frac{d}{dt} (n_j k T_j) = P_{\alpha j} - \frac{3}{2} \frac{n_j k T_j}{\tau_{Ej}} - \frac{3}{2} n_j k \left(\frac{T_j - T_e}{\tau_{je}^{eq}} + \sum_J \frac{T_j - T_J}{\tau_{jJ}^{eq}} \right). \quad (6.4-12)$$

Here $P_{\alpha j}$ is the power deposited into ion species "j" by energetic α particles as they slow down (Section 6.4.3), τ_{Ej} is the energy confinement time and summation on "J" is carried over all ion species. The energy equilibration time between Maxwellian species "j" and "s," τ_{js}^{eq} , is given by

$$\tau_{js}^{eq} = \frac{3\sqrt{2\pi^3} \epsilon_0}{e^4} \frac{m_j m_s}{Z_j^2 Z_s^2 \lambda_{js}} \left(\frac{kT_j}{m_j} + \frac{kT_s}{m_s} \right)^{3/2}, \quad (6.4-13)$$

where λ_{js} is the coulomb logarithm, Z_j and m_j are, respectively, the atomic number and the mass of species "j," k is the Boltzmann constant, and ϵ_0 is the permittivity of free space.

The electron power balance equation is

$$\frac{3}{2} \frac{d}{dt} (n_e k T_e) = P_{\alpha e} + P_{OHM} - P_{RAD} - \frac{3}{2} \frac{n_e k T_e}{\tau_{Ee}} - \frac{3}{2} \sum_J n_e k \left(\frac{T_e - T_J}{\tau_{eJ}^{eq}} \right), \quad (6.4-14)$$

where P_{RAD} is the radiative power loss. The ohmic heating power into the plasma, P_{OHM} , is

$$P_{OHM} = \frac{2}{r_p^2} \int_0^{r_p} \eta_{\parallel}(r) J_{\parallel}^2(r) r dr, \quad (6.4-15)$$

where η_{\parallel} , the classical resistivity of the plasma, is

$$\eta_{\parallel} = 0.51 \frac{4\sqrt{2\pi}}{3} \frac{m_e^{1/2}}{k^{3/2}} \left(\frac{e}{4\pi\epsilon_0} \right)^2 \frac{Z_{eff}}{N(Z_{eff})} \lambda_{ei} T_e^{-3/2}(r), \quad (6.4-16)$$

$$N(Z_{eff}) \simeq 1 + 0.718 \left(\frac{Z_{eff} - 1}{Z_{eff}} \right)^2. \quad (6.4-17)$$

The plasma-resistance composite-profile factor, g_{OHM} , which includes the effect of the temperature profile as well as the field-line screw-up factor, was defined in Section 5.2 such that

$$P_{OHM} = g_{OHM} \langle \eta_{\parallel} \rangle \langle J_{\parallel} \rangle^2, \quad (6.4-18)$$

where $\langle \eta_{\parallel} \rangle$ is the classical resistivity computed by using the average electron temperature, T_e . The parameter g_{OHM} includes all profile information, is independent of plasma current and size, and only depends on the plasma profiles (μ , n , and T), β_{θ} , and F or Θ values (Section 5.2). For $F = -0.1$ and power profiles (Equations 6.4-3 through 6.4-5), g_{OHM} ranges from 4.0 to 3.4 as β_{θ} is increased from 0. to 0.2.

The radiative power loss from plasma, P_{RAD} , includes bremsstrahlung, synchrotron, and line radiation losses. For the TITAN plasma, synchrotron radiation losses are usually very small. The burning TITAN plasma is deliberately doped with xenon impurities to spread the plasma losses uniformly over the first wall, which reduces the heat load to the divertor plates. In this case, most of the plasma power is radiated in the form of line radiation caused by xenon impurities (Section 5.3). These impurities, however, are introduced into the plasma after the ignition phase in order to reduce the time and energy needed to achieve ignition and steady-state burn. Therefore, line radiation is ignored during start-up transient simulations. The radiative power, therefore, is mostly by bremsstrahlung,

$$P_{RAD} \simeq P_{brem} = 4.23 \times 10^{-29} g_{brem} n_e^2 Z_{eff} (kT_e)^{1/2}, \quad (6.4-19)$$

where g_{brem} is the bremsstrahlung profile factor,

$$g_{brem} \equiv \frac{2}{r_p^2} \int_0^{r_p} \hat{n}_e^2(r) \hat{T}_e^{1/2}(r) r dr. \quad (6.4-20)$$

The parameter, g_{brem} depends only on the profiles of electron density [$\hat{n}_e \equiv n_e(r)/n_e(0)$] and temperature [$\hat{T}_e \equiv T_e(r)/T_e(0)$]. For power profiles (Equations 6.4-3 through 6.4-5), $g_{brem} = 1.329$ and for radiative profiles (Equations 6.4-6 through 6.4-8), $g_{brem} = 1.172$.

The reactivity profile factors, g_{DT} , can be defined in the same manner,

$$g_{DT} = \frac{2}{r_p^2} \int_0^{r_p} \hat{n}_D(r) \hat{n}_T(r) \frac{\langle \sigma v \rangle [T_i(r)]}{\langle \sigma v \rangle (T_i)} r dr, \quad (6.4-21)$$

where \hat{n} is the normalized density profile and $\langle \sigma v \rangle (T_i)$ is DT reactivity computed for the plasma average temperature, T_i , while $\langle \sigma v \rangle [T_i(r)]$ is the local DT reactivity. Then, the α -particle power, P_α , is

$$P_\alpha = k E_\alpha g_{DT}(T_i) n_D n_T \langle \sigma v \rangle (T_i), \quad (6.4-22)$$

where $E_\alpha = 3.52$ MeV is the birth energy of α particles. Note that g_{DT} is a function of average temperature, T_i .

Finally, the RFP electron energy-confinement time, τ_{Ee} , is assumed to scale from values obtained in present-day experiments (Section 2.3.5) according to

$$\tau_{Ee} = C_\nu I_\phi^\nu r_p^2 f(\beta_\theta), \quad (6.4-23)$$

with typical values of the current scaling exponent, ν , and the corresponding numerical coefficient, C_ν , summarized in Table 6.4-I and Figure 2.3-20 for $\tau_{Ei} = 4 \tau_{Ee}$. The function $f(\beta_\theta)$ models the soft β limit and is assumed to have a value of one for β values below the β limit, $\beta_{\theta c}$, and to go to zero when the β limit value is exceeded. For TITAN transient analyses, a value of $\nu = 0.05$ is used and $f(\beta_\theta)$ is modeled by a Fermi-Dirac probability function,

$$f(\beta_\theta) = \left[1 + \exp \left(\alpha \frac{\beta_\theta - \beta_{\theta c}}{\beta_{\theta c}} \right) \right]^{-1}, \quad (6.4-24)$$

with $\alpha = 50$ and $\beta_{\theta c} = 0.22$.

6.4.3. Energetic Alpha Particles

The distribution function of the fusion product “a” (*e.g.*, α particles) in the plasma can be found using the Fokker-Planck equation, which for isotropic distribution functions is given by

$$\frac{\partial f_a}{\partial t} = \sum_s \frac{1}{v^2} \frac{\partial}{\partial v} \left[\mathcal{P}_{as}(v) \frac{\partial f_a}{\partial v} + \mathcal{Q}_{as}(v) f_a(v) \right] + S_a(v) - L_a(v). \quad (6.4-25)$$

Table 6.4-I.
RFP ELECTRON ENERGY-CONFINEMENT
SCALING PARAMETERS^(a)

ν	C_ν (s/m ² -MA ^{ν})
1.50	0.1400
1.40	0.1140
1.25	0.0837
1.20	0.0614
1.10	0.0620
1.05	0.0554
1.00	0.0500
0.90	0.0407
0.80	0.0331

$$(a) \tau_E \equiv 2(1/\tau_{Ee} + 1/\tau_{Ei})^{-1},$$

$$\tau_{Ee} = C_\nu I_\phi^\nu r_p^2, \tau_{Ei} = 4\tau_{Ee}.$$

Here, the summation is carried out over all plasma species (*i.e.*, electrons, ions, and fusion products), S_α is the source of fast particles (*e.g.*, fusion products), L_α is the fast-particle loss term,

$$L_\alpha(v) = \frac{f_\alpha(v)}{\tau_{pa}}, \quad (6.4-26)$$

τ_{pa} is the fast-particle confinement time, and \mathcal{P} and \mathcal{Q} are given by

$$\mathcal{P}_{\alpha s} = \frac{4\pi}{3} \Gamma_{\alpha s} \left[\int_0^v f_s(u) u^4 du + v^2 \int_v^\infty f_s(u) u du \right], \quad (6.4-27)$$

$$\mathcal{Q}_{\alpha s} = 4\pi \frac{m_\alpha}{m_s} \Gamma_{\alpha s} \int_0^v f_s(u) u^2 du, \quad (6.4-28)$$

where

$$\Gamma_{as} = \frac{4}{\pi} \left(\frac{Z_a Z_b e^2}{4\pi \epsilon_0} \right)^2 \lambda_{as}. \quad (6.4-29)$$

The density and pressure of fusion products, then, can be found from $f_a(v)$:

$$n_a = 4\pi \int_0^\infty f_a(v) v^2 dv, \quad (6.4-30)$$

$$p_a = \frac{4\pi m_a}{3} \int_0^\infty f_a(v) v^4 dv. \quad (6.4-31)$$

The power transfer due to collisions from species "a" to species "s" is

$$P_{as} = 4\pi m_a \int_0^\infty \left[\mathcal{P}_{as}(v) + v \frac{d\mathcal{P}_{as}}{dv} - v \mathcal{Q}_{as}(v) \right] f_a(v) dv. \quad (6.4-32)$$

If species "s" has a Maxwellian distribution, $f_s(v) = (n_s/\pi^{3/2}v_s^3) \exp(-v^2/v_s^2)$, \mathcal{P}_{as} and \mathcal{Q}_{as} can be written as

$$\mathcal{P}_{as}(v) = \frac{2}{\sqrt{\pi}} n_s v_s \Gamma_{as} G(v/v_s), \quad (6.4-33)$$

$$\mathcal{Q}_{as}(v) = \frac{2}{\sqrt{\pi}} n_s v_s \Gamma_{as} \frac{2m_a}{m_s} G(v/v_s), \quad (6.4-34)$$

$$\mathcal{P}_{as} + v \frac{d\mathcal{P}_{as}}{dv} = \frac{2}{\sqrt{\pi}} n_s v_s \Gamma_{as} \left(\frac{v}{v_s} \right)^2 \exp\left(-\frac{v^2}{v_s^2}\right), \quad (6.4-35)$$

where $v_s = \sqrt{2kT_s/m_s}$ is the thermal speed of species "s,"

$$G(x) \equiv \frac{\sqrt{\pi}}{4x} \operatorname{erf}(x) - \frac{1}{2} \exp(-x^2), \quad (6.4-36)$$

and $\operatorname{erf}(x)$ is the error function.

For the TITAN transient simulations, Equation 6.4-25 is solved using the numerical method of Reference [14], which is an extension of Chang and Cooper technique [15]. Equation 6.4-25 is nonlinear (functions \mathcal{P}_{aa} and \mathcal{Q}_{aa} depend on f_a). Therefore, at each time step, an iteration scheme over the distribution function of fast species, f_a , were used: \mathcal{P} and \mathcal{Q} functions are evaluated using the old values of f_a , new values for f_a are calculated based on these \mathcal{P} and \mathcal{Q} functions, these new values of f_a are used to update \mathcal{P} and \mathcal{Q} functions, and f_a values are again updated until convergence is achieved. The distribution of background plasma species are assumed to be Maxwellian. Because the ion temperature is much smaller than the fusion α -particle birth energy ($T_i \ll E_\alpha$), the α -particle source is assumed to be a delta function at energy E_α .

6.4.4. Ignition Analysis

The steady-state analysis of global plasma power balance provides useful information for the optimization of plasma approach to ignition. Results of this type of analysis for auxiliary-heated fusion devices are usually presented in the form of required auxiliary power for power balance as a function of plasma density and temperature. This information is then used to identify the path to ignition that requires minimum auxiliary heating power. Similar analysis can be applied to compact RFP reactors in which the plasma is heated to ignition by ohmic heating alone (no auxiliary heating).

Addition of the ion and electron power-balance equations (Equations 6.4-12 and 6.4-14) for steady state results in

$$\frac{3}{2} \left(\frac{n_e T_e}{\tau_{Ee}} + \sum_j \frac{n_j T_j}{\tau_{Ej}} \right) = P_\alpha + P_{OHM} - P_{RAD}, \quad (6.4-37)$$

where P_{OHM} , P_{RAD} , and P_α are given, respectively, by Equations 6.4-18, 6.4-19, and 6.4-22. Equation 6.4-37 can be solved for the required plasma current for power balance, I_ϕ , as a function of density and temperature for a given plasma size, ion mixture, plasma profiles (n , T , and μ), F or Θ values, and the scaling of τ_E as given by Equation 6.4-23 and 6.4-24 (current exponent, ν , and the soft β limit, $\beta_{\theta c}$). Because of the high density of RFP plasmas, the electron/ion energy-equilibration time, τ_{ei}^{eq} , is short resulting in $T_e \simeq T_i \simeq T$.

Results of this analysis for the TITAN plasma ($r_p = 0.6$ m) are shown in Figure 6.4-1 for a 50:50 DT mixture, $n_e \simeq n_i \simeq n$ ($Z_{eff} = 1$), plasma power profiles (Equations 6.4-3 through 6.4-5), and $F = -0.1$. A current exponent of $\nu = 1.05$ and a soft β limit of $\beta_{\theta c} = 0.23$ are used. Figure 6.4-1(A) shows a "ridge" in the I_ϕ - n - T space above which the path to ignition and burn should be located (similar to corresponding diagrams for auxiliary heated devices where a ridge for auxiliary heating exists). The optimum ignition scenario attempts to pass over the ridge at its lowest height (saddle point). This saddle point, which is denoted by a filled circle in the figure, is at $T \simeq 7$ keV and $n \simeq 3 \times 10^{20} \text{ m}^{-3}$ with a current of $I_\phi \simeq 16$ MA. The TITAN start-up path through ignition and burn passes close to this saddle point (Section 6.5.3).

The corresponding contours of constant I_ϕ are shown in Figure 6.4-1(B). The chain dashed line in this figure is the contour of $\beta_\theta = 0.2$ and the points above this line all have β values of ~ 0.2 because of the assumption of the β -limited confinement. This point is emphasized in Figure 6.4-2, which illustrates the β_θ corresponding to I_ϕ values of Figure 6.4-1. The flat part of the β_θ surface at high T and n represent the operating

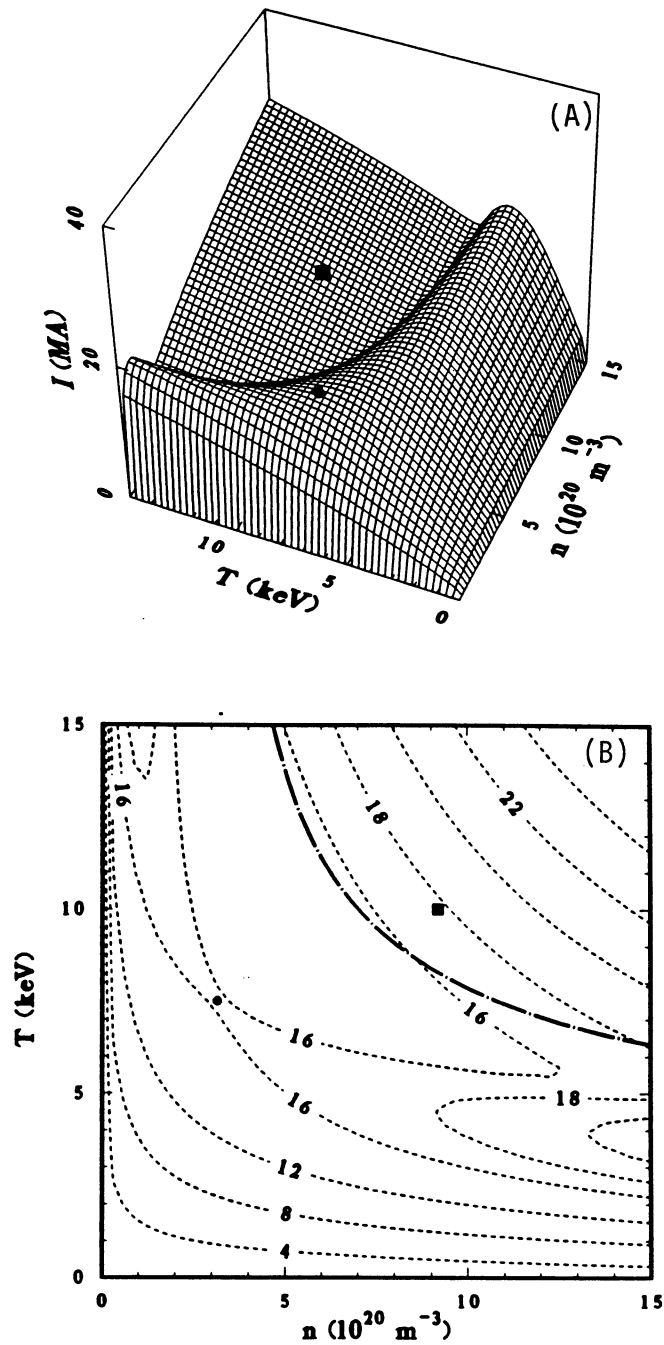


Figure 6.4-1. The required current for power balance as a function of TITAN plasma density and temperature (A) and the corresponding contour plot (B). The steady-state TITAN plasma is denoted by a filled square and the saddle point by a filled circle. The path to ignition and burn should be located above this surface.

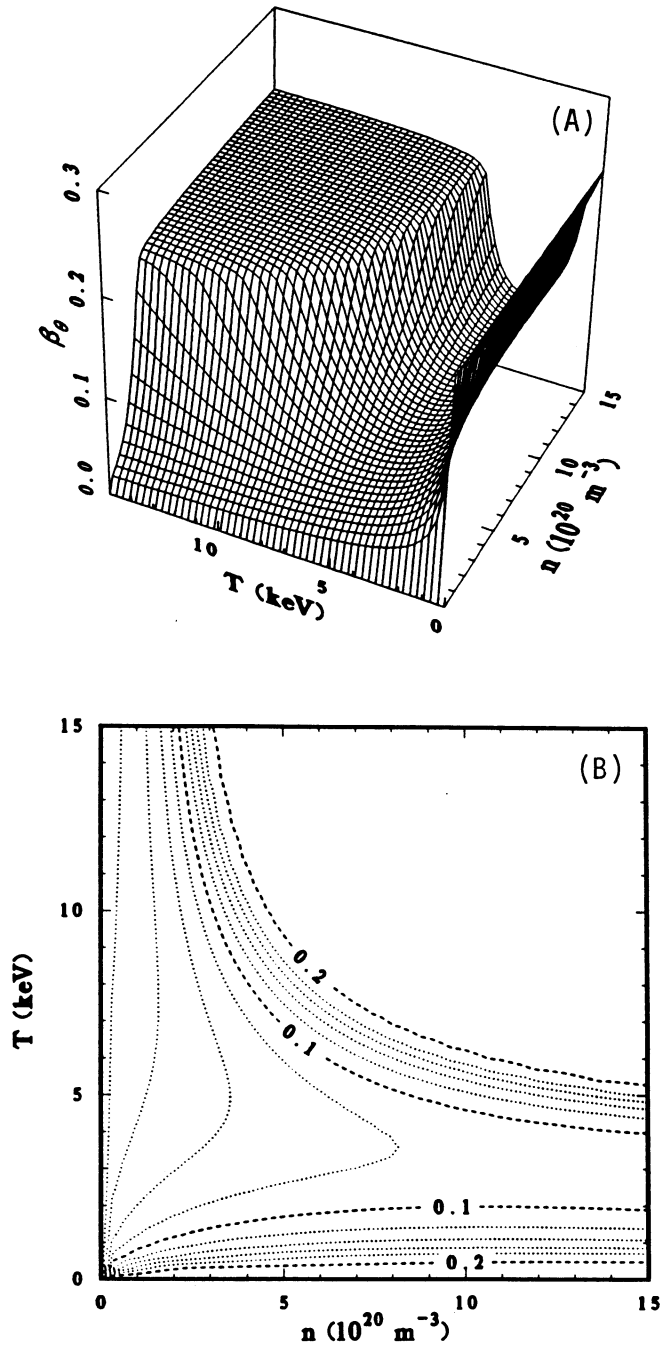


Figure 6.4-2. The plasma β corresponding to the required current for power balance as a function of TITAN plasma density and temperature (A) and the corresponding contour plot (B). The flat portion of the β_{θ} surface is due to the β -limited confinement assumption. The path to ignition and burn should be located below this surface.

point at the β limit. Note that the path to ignition should stay below this β_θ surface since it should stay above the current surface of Figure 6.4-1. The β_θ value for the saddle point is about 7%.

The sensitivity of the structure of the I_ϕ - n - T ignition surface to the various assumptions has been also studied. The β -limited confinement assumption does affect the ridge structure and only changes the current values above the chain-dashed line of Figure 6.4-1. If the confinement scaling is more favorable with current (higher ν values), the saddle point moves towards lower currents and slightly lower densities. For example, for $\nu = 1.2$, the current is reduced to 12 MA. Increasing Z_{eff} from 1.0 to 1.7, increases the current by about 10% and electron density by 50% (note that line radiation is ignored).

6.5. CURRENT RAMP-UP TO IGNITION AND BURN

The TITAN start-up scenario through current ramp, ignition, and burn transients is chosen such that the start-up power is directly extracted from the power grid without requiring an on-site power-storage system. This start-up scenario is described in Section 6.5.1 and its implications for the poloidal-field-coil system are reviewed. The evolution of the TITAN plasma through the start-up sequence is investigated by using a 0-D, profile-averaged plasma-circuit code. The plasma models were described in Section 6.4. The circuit model for the plasma, the poloidal-field (PF) system, and the eddy currents in the FPC are reviewed in Section 6.5.2. A description of the plasma-circuit code as well as the simulation results are presented in Section 6.5.3.

6.5.1. Start-Up Sequence

The current in the TITAN plasma is initiated and then ramped to full value through induction by the PF-coil system. In addition to producing the required flux change, the PF system must also generate the necessary equilibrium-field distribution. The most efficient way to produce a net flux change is through bipolar operation of the coil system since the stored energy, magnetic-field strength, coil stress, and joule losses would be minimized. Plasma equilibrium depends on the magnitude of the plasma current and the equilibrium field produced by the PF coils should closely match the required vertical field for equilibrium.

For the TITAN designs, the PF-coil system is divided into two sets of coils: the ohmic-heating (OH) coil set, which produces most of the flux swing but does not produce any

equilibrium (vertical) field; and the equilibrium-field (EF) coil set, which produces the necessary vertical field and may or may not contribute to the flux swing. This approach allows the OH coils to be operated independently of the magnitude of the plasma current. Furthermore, we will show that the magnetic properties of the OH- and EF-coil sets and the start-up switching sequence can be chosen such that the EF coil produces the required vertical field approximately, without any need for a highly controlled power supply for the EF coils.

The TITAN-I start-up scenario is chosen such that the start-up power is directly extracted from the power grid without requiring an on-site power-storage system (other than the coils themselves). The start-up switching sequence is shown in Figure 6.5-1. An illustration of the corresponding current and voltage waveforms are given in Figure 6.5-2. The TITAN start-up sequence uses a bipolar swing of the OH-coil currents and begins with charging the OH coils to their full back-bias values. The OH coils are then discharged into a transfer resistor, while the EF coils are connected in parallel to the OH coils ("formation and fast discharge" phase in Figures 6.5-1 and 6.5-2). The value of the transfer resistor is set by the constraint on the maximum voltage across the superconducting EF coils. The fast-discharge phase lasts about 1 to 2 seconds.

As the OH coils are discharging, the voltage across the circuit drops. When the voltage across the OH coils reaches that of the grid power supply, the transfer resistor is disconnected from the circuit and the grid power supply is directly applied to the OH and EF coils ("slow-ramp" phase). The OH coils are driven to their full, forward-bias current value and the EF coils and the plasma to their respective steady-state currents. The voltage of the grid power supply is usually a few kilovolts and its value is determined by the maximum power from the grid. The current-drive system begins operation during this phase and will be fully operational at the burn phase, maintaining the steady-state current in the plasma. After achieving the steady-state burn condition, the OFCD system is initiated while the OH coils are discharged slowly, from the full forward-bias current value to zero, in order to minimize the recirculating power and the coil-cooling requirements. Initiation of OFCD operation during the slow-ramp phase is advantageous.

With the proper magnetics design of the OH and EF coils, this start-up scenario will provide approximate plasma equilibrium throughout the start-up sequence. To find the magnetics design requirements, we consider the fast- and slow-ramp phases of the start-up sequence (Figure 6.5-1). Ignoring the trim-coil circuit and eddy currents that may be induced in the fusion power core (FPC), the circuit equations for the plasma and

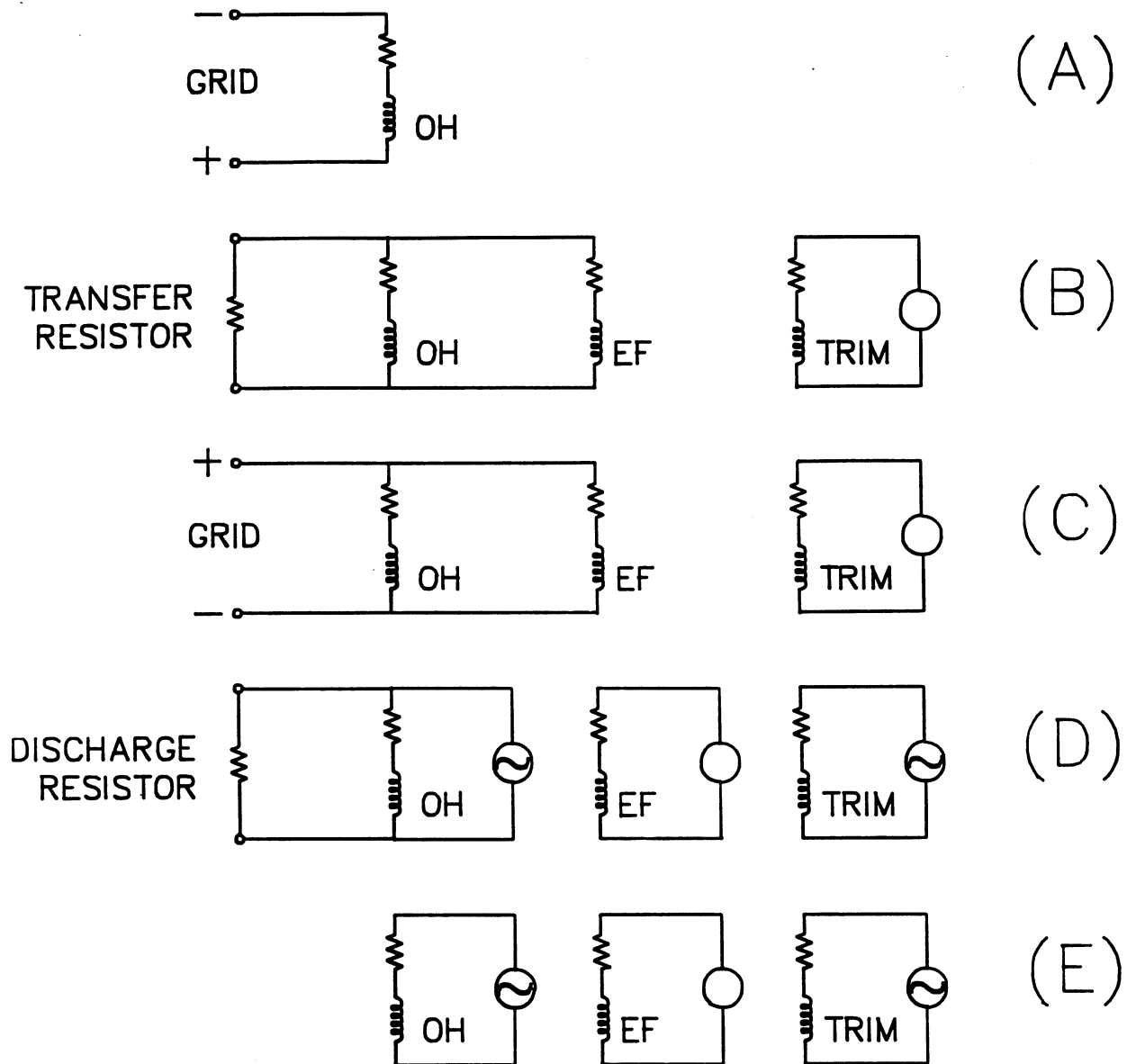


Figure 6.5-1. Start-up sequence for the TITAN reactors: (A) Charge-up – OH coils are charged to full back-bias value, (B) Formation and fast discharge – OH coils are discharged through a transfer resistor (EF coils are connected in parallel to the OH coils), (C) Slow ramp – grid power drives the OH coils to full forward bias: current and the EF coils to their steady-state value, (D) Transition – the OH coils are slowly discharged while OFCD is initiated, and (E) Steady state – current-drive system is fully operational. Initiation of OFCD operation during the slow-ramp phase is advantageous.

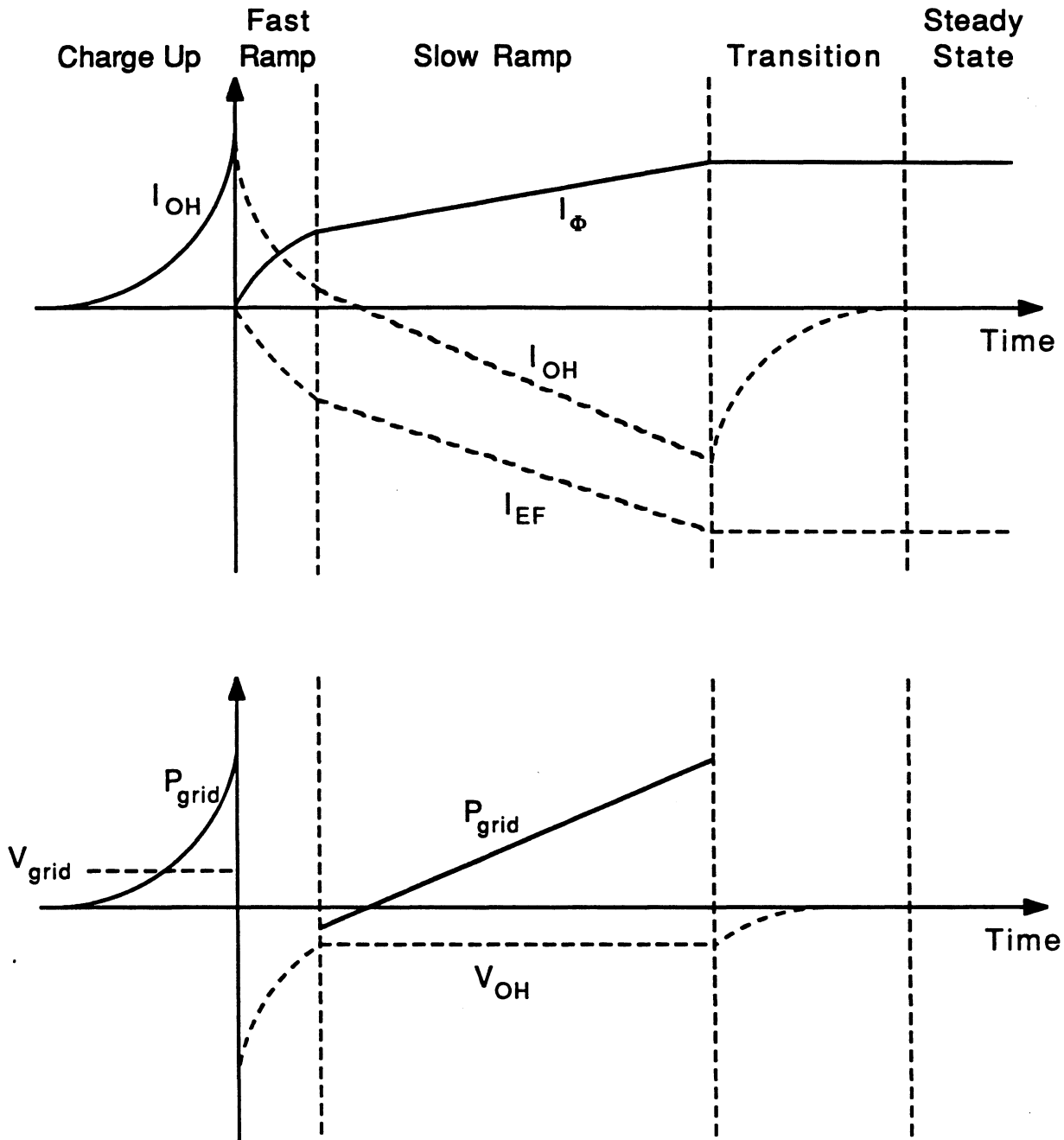


Figure 6.5-2. Schematic of coil currents and voltages during the TITAN start-up sequence corresponding to Figure 6.5-1: (A) Charge-up, (B) Formation and fast-discharge, (C) Slow-ramp, (D) Transition, and (E) Steady-state phases. Note that the time axis is not in scale.

the OH and EF coils are, respectively,

$$L_p \frac{dI_\phi}{dt} + M_{OH,p} \frac{dI_{OH}}{dt} + M_{EF,p} \frac{dI_{EF}}{dt} = -R_p I_\phi, \quad (6.5-1)$$

$$M_{OH,p} \frac{dI_\phi}{dt} + L_{OH} \frac{dI_{OH}}{dt} + M_{EF,OH} \frac{dI_{EF}}{dt} = \frac{v_{OH}}{N_{OH}} - R_{OH} I_{OH}, \quad (6.5-2)$$

$$M_{EF,p} \frac{dI_\phi}{dt} + M_{EF,OH} \frac{dI_{OH}}{dt} + L_{EF} \frac{dI_{EF}}{dt} = \frac{v_{EF}}{N_{EF}} - R_{EF} I_{EF}, \quad (6.5-3)$$

where the direction of the plasma current is taken to be the positive direction for the current in all circuits, L and M represent equivalent single-turn inductances, currents are given in Ampere-turn, and N denotes the number of turns in each coil set. Eliminating I_{OH} from Equations 6.5-1 through 6.5-3 and noting that $v_{OH} = v_{EF}$ during both fast- and slow-ramp phases, one has

$$\begin{aligned} & \left[\frac{N_{OH}}{N_{EF}} (M_{OH,p}^2 - L_{OH} L_p) - (M_{OH,p} M_{EF,p} - M_{OH,EF} L_p) \right] \frac{dI_\phi}{dt} + \\ & \left[\frac{N_{OH}}{N_{EF}} (M_{OH,p} M_{OH,EF} - L_{OH} M_{EF,p}) - (M_{OH,p} L_{EF} - M_{OH,EF} M_{EF,p}) \right] \frac{dI_{EF}}{dt} \\ = & R_p I_\phi \left(\frac{N_{OH}}{N_{EF}} L_{OH} - M_{OH,EF} \right) - M_{OH,p} \left(\frac{N_{OH}}{N_{EF}} R_{OH} I_{OH} - R_E I_E \right). \end{aligned} \quad (6.5-4)$$

If the resistances are ignored (circuit L/R time is much longer than start-up duration), Equation 6.5-4 can be integrated subject to the initial condition of $I_\phi = I_{EF} = 0$ at time $t = 0$ to get

$$-\frac{I_{EF}}{I_\phi} = \frac{\frac{N_{OH}}{N_{EF}} (M_{OH,p}^2 - L_{OH} L_p) - (M_{OH,p} M_{EF,p} - M_{OH,EF} L_p)}{\frac{N_{OH}}{N_{EF}} (M_{OH,p} M_{OH,EF} - L_{OH} M_{EF,p}) - (M_{OH,p} L_{EF} - M_{OH,EF} M_{EF,p})}. \quad (6.5-5)$$

For a fixed PF-coil set, the vertical field produced by the EF coils directly scales with the EF current, while the vertical field necessary for plasma equilibrium scales directly with I_ϕ . Hence, the needed ratio of the final EF-coil current to the final plasma current, $-I_{EF}^+/I_\phi^+ = |I_{EF}^+/I_\phi^+|$, and the single-turn inductances are known. Equation 6.5-5 can then be used to find the value of N_{OH}/N_{EF} so that the proper equilibrium is maintained during the discharge:

$$\frac{N_{OH}}{N_{EF}} = \frac{M_{OH,EF}(C_1 - C_3)}{L_{OH}(C_1 - C_2)}, \quad (6.5-6)$$

where

$$C_1 \equiv \frac{1}{M_{OH,p}} \left(L_p - M_{EF,p} \left| \frac{I_{EF}^+}{I_\phi^+} \right| \right), \quad (6.5-7)$$

$$C_2 \equiv \frac{1}{L_{OH}} \left(M_{OH,p} - M_{OH,EF} \left| \frac{I_{EF}^+}{I_\phi^+} \right| \right), \quad (6.5-8)$$

$$C_3 \equiv \frac{1}{M_{OH,EF}} \left(M_{EF,p} - L_{EF} \left| \frac{I_{EF}^+}{I_\phi^+} \right| \right). \quad (6.5-9)$$

Parameters C_1 through C_3 reflect the degree of coupling between various circuit elements.

Since the eddy current induced in the FPC and resistances in various circuits are ignored in arriving at Equation 6.5-5, the equilibrium provided by the EF coils during the start-up sequence is an approximate equilibrium. The TITAN PF-coil system, therefore, includes a pair of small, normal-conducting trim coils to maintain exact equilibrium during the start-up sequence. Using this approach, only the power supplies for the EF trim coils have to be feedback controlled to ensure proper equilibrium. The EF trim coils are also used during the steady-state operation for plasma equilibrium control and OFCD cycles (Section 7).

The magnetics design of the PF-coil systems for the TITAN designs is given in Section 4.5 and magnet engineering issues are discussed in Section 10.5. The relevant circuit parameters for the TITAN PF coils are given in Table 6.5-I.

6.5.2. Circuit Model

The time-varying electromagnetic fields incurred during the plasma transients induce eddy currents in all the conducting materials surrounding the FPC (*i.e.*, those of the first wall, liner/conducting shell, vacuum vessel, blanket, shield, and structures). These eddy currents retard and modify the plasma response to externally applied magnetic fields. Furthermore, these eddy currents give rise to magnetic fields affecting the plasma equilibrium, to electromagnetic forces on all conducting materials that carry the eddy currents, and to an additional energy drain from the external circuits to compensate for joule losses by eddy currents. Eddy-current modeling is, therefore, critical and it is usually the most difficult task in plasma-circuit interaction analysis. The approach to this problem, adopted for the TITAN study, is to divide the conducting material into small strips that simulate the actual eddy-current path and distribution. Each strip is modeled as an element of a complex circuit that also includes the external circuitry

Table 6.5-I.
CIRCUIT PARAMETERS FOR TITAN PF-COIL DESIGNS^(a)

	TITAN-I	TITAN-II
Self inductances (μH)		
· L_p	13.29	13.29
· L_{OH}	2.74	3.68
· L_{EF}	15.02	13.35
· L_{Trim}	18.36	19.35
Mutual inductances (μH)		
· $M_{OH,p}$	2.87	3.92
· $M_{OH,EF}$	2.26	3.04
· $M_{OH,Trim}$	2.99	4.03
· $M_{EF,p}$	3.86	4.12
· $M_{EF,Trim}$	8.69	8.22
· $M_{Trim,p}$	5.60	6.15
Current levels (MA-turn)		
· I_ϕ	17.75	17.82
· I_{EF}	19.24	18.60
· ΔI_{OH}	55.80	40.82
Magnetic fluxes (Wb)		
· Plasma	236.0	236.9
· EF coil	74.5	77.1
· OH coil	161.5	159.8

(a) Equivalent single-turn inductance values are given.

and an equivalent circuit element for the plasma. The interaction of these elements is taken into account through the circuit-inductance matrix, \mathbf{L} , containing self- and mutual inductances for all elements. The matrix circuit equation describing the evolution of currents in various circuit elements is

$$\frac{d}{dt}(\mathbf{L} \cdot \mathbf{I}) = \mathbf{V} - \mathbf{R} \cdot \mathbf{I}, \quad (6.5-10)$$

where \mathbf{I} and \mathbf{V} are column vectors of currents (Ampere-turn) and voltages (volt/turn) and \mathbf{R} is the diagonal matrix of resistances. For a given time history of voltages and switching sequences, the above matrix equation can be solved to obtain the currents and, then, magnetic fields and power flow through the circuits. In principle, the accuracy of such a procedure should be improved by increasing the number of the equivalent eddy-current circuit elements, which, in turn, increases the complexity of the overall circuit analysis as well as the computation time.

The starting point of this procedure is the division of the conducting material into equivalent eddy-current circuit elements. Such a division, however, requires *a priori* knowledge of eddy-current paths and distributions. Furthermore, introducing resistive breaks to suppress the magnitude of eddy currents and associated effects results in "saddle" current loops. Circuit simulations for the TITAN start-up transient analysis is limited to the equivalent circuits for the poloidal field. Each eddy-current path is approximated by a toroidal "conductor" model, whereas the effect of the resistive breaks is modelled only as a dramatic increase in the resistance of the eddy-current circuit. The poloidal component of the saddle current loops that impacts the toroidal-field system is ignored. Note that both poloidal and toroidal components of saddle loop currents are included in the circuit simulation of OFCD of Section 7.

Special attention is also given to the EF-coil circuits. At all times, the current in the EF coils should provide the necessary vertical field to maintain the plasma equilibrium. The required value of this vertical field at the magnetic axis is given by Shafranov [16]:

$$B_V = \frac{\mu_0 I_\phi}{4\pi R_T} \left[\ln \left(\frac{8R_T}{r_p} \right) + \beta_\theta + \frac{l_i}{2} - 1.5 \right], \quad (6.5-11)$$

where l_i is the plasma internal inductance per unit length. It has been shown [17] that the Shafranov formula is an accurate measure of the required vertical field for an RFP over a wide range of plasma conditions. In the presence of conducting material, the vertical field produced by the EF coils, together with contributions from other external coils and eddy currents, should be equal to the vertical field given by Equation 6.5-11:

$$\sum_{j \neq \text{plasma}} (B_z)_j = B_V, \quad (6.5-12)$$

where $(B_z)_j$ is the vertical field produced by circuit “j” and B_V is the required vertical field. Since $(B_z)_j \propto I_j$ and $B_V \propto I_p$, Equation 6.5-12 can be written as

$$\sum_{j \neq \text{plasma}} c_j I_j + c_p I_p = 0, \quad (6.5-13)$$

where $c_p \equiv -B_V/I_p$ can be found from Equation 6.5-11 and constants c_j depend only on coil or conductor geometry and location. Taking the time derivative of Equation 6.5-13, one finds

$$\frac{d}{dt} \left(\sum_j c_j I_j \right) = 0, \quad (6.5-14)$$

where the summation is over all circuits (including the plasma).

6.5.3. Plasma-Circuit Simulations

The evolution of the TITAN plasma through current ramp, ignition, and burn transients is investigated by using a 0-D, profile-averaged plasma-circuit code. The plasma profiles (n , T , and μ) used in the transient analyses are the power profiles given by Equations 6.4-3 through 6.4-5. Equilibrium calculations of Section 5.2 are used to compute the plasma-resistance composite-profile factor, g_{OHM} , and the plasma internal inductance per unit length, l_i . It is shown in Section 5.2 that these two parameters are independent of plasma current and size, and only depend on the plasma profiles, β_θ , and F or Θ values. It is assumed that the value of F is held constant during start-up transients by proper programming and/or feedback control of the TF coils at $F = -0.1$. Therefore, g_{OHM} and l_i change only in response to change in β_θ during the start-up transients, as is shown in Figure 6.5-3. To save computational time, a table for values of g_{OHM} and l_i as functions of β_θ is made at the start of the calculations and the necessary values at each time are found through interpolation.

The plasma-circuit simulation code solves the ion and electron power-balance equation (Section 6.4.2) and the Fokker-Planck equation for fusion α particles (Section 6.4.3) using an implicit time-differencing scheme. The desired evolution of the plasma density, obtained from the ignition requirement analysis of Section 6.4.4, is used together with the particle balance equation (Equation 6.4-9) to determine the required fueling rate. Between each time step, a circuit-analysis package integrates the circuit equations using an adaptive Rung-Kutta method [18]. At the start of the analysis and for the given FPC geometry and external coil sets, the code divides the FPC into small sectors and

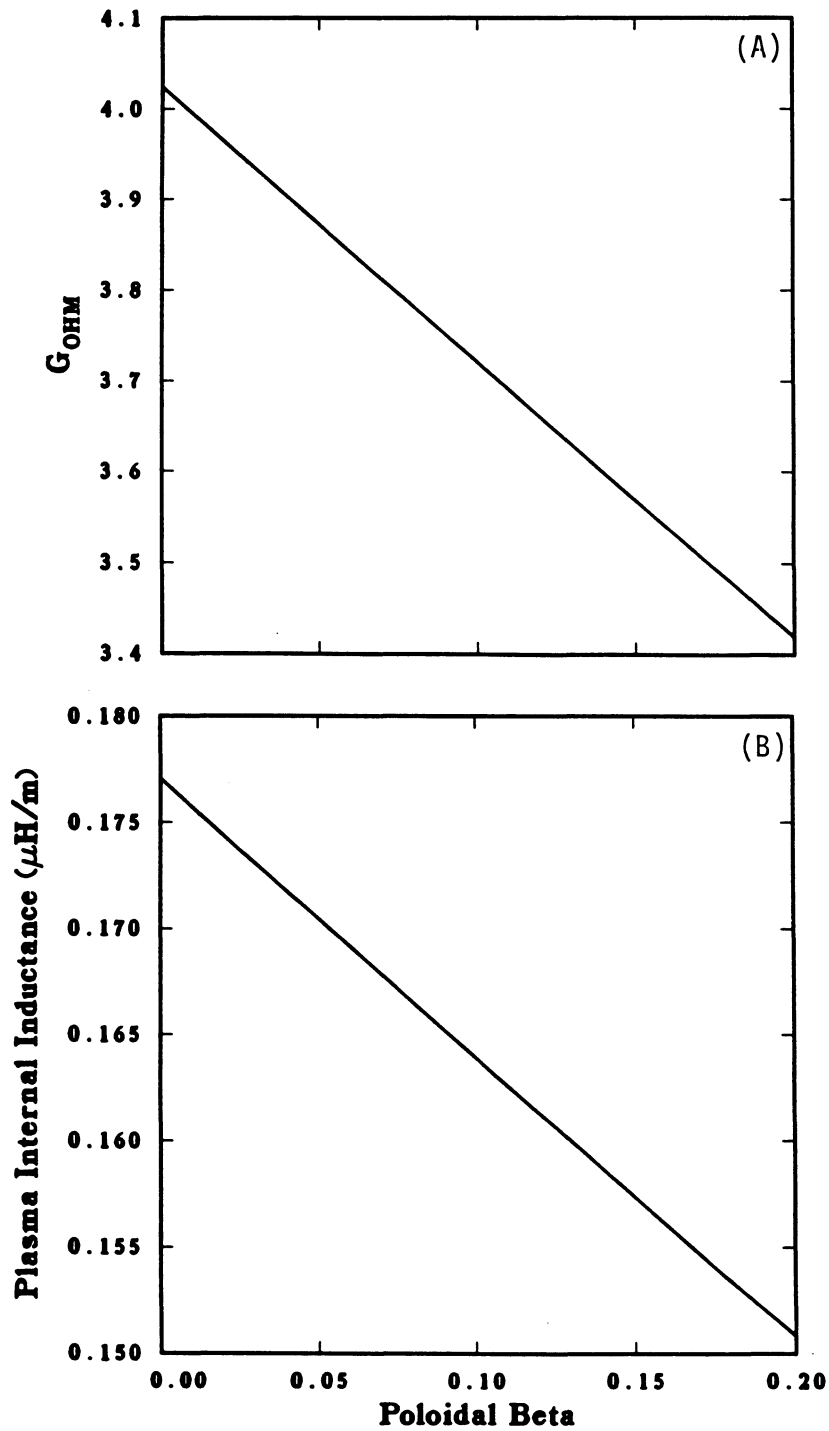


Figure 6.5-3. The plasma-resistance composite-profile factor (A) and the plasma internal inductance per unit length (B) as functions of β_θ for $F = -0.1$ and power profiles (Equations 6.4-3 through 6.4-5).

models each as an eddy-current circuit element. The self- and mutual inductances of the various circuit elements are then calculated (as described in Section 4.5), and the overall inductance matrix is constructed.

Ignoring changes in the plasma position during the start-up transients, only the plasma inductance in the circuit inductance matrix changes in time since plasma internal inductance changes as β_θ evolves. Including the \dot{L}_p term in the plasma resistance, the circuit equation (Equation 6.5-11) can be written as

$$\dot{\mathbf{I}} = \mathbf{L}^{-1} \cdot (\mathbf{V} - \mathbf{R} \cdot \mathbf{I}), \quad (6.5-15)$$

where \mathbf{L}^{-1} is the inverse of the inductance matrix. Because the plasma inductance changes, a new \mathbf{L}^{-1} should be computed at each time step. Instead of inverting \mathbf{L} at each time step, however, one can use the Sherman-Morrison formula [18] to find \mathbf{L}^{-1} since only one element of \mathbf{L} changes. A special case of this formula for matrices \mathbf{L} and \mathbf{L}^* , which are identical except in element L_{11} , is

$$L_{ij}^{*-1} = L_{ij}^{-1} - \frac{L_{i1}^{-1} L_{1j}^{-1} (L_{11}^* - L_{11})}{1 + L_{11}^{-1} (L_{11}^* - L_{11})}. \quad (6.5-16)$$

The TITAN PF-coil system includes a pair of EF trim coils to provide the exact equilibrium through the plasma transient operations. The code computes the necessary voltage that should be applied to the trim coils through the following procedure: Denoting $\dot{\mathbf{I}}^*$ as the solution to Equation 6.5-15 for $v_{Trim} = 0$, then

$$\dot{I}_i = \dot{I}_i^* + L_{i,Trim}^{-1} \frac{v_{Trim}}{N_{Trim}}. \quad (6.5-17)$$

Substituting the above equation in Equation 6.5-14 results in a first order equation in v_{Trim} that can be solved to find the necessary voltage that should be applied to the EF trim circuit. The same procedure can also be applied when the main EF coils reach their steady-state value and are crowbarred ($\dot{I}_{EF} = 0$), and when the plasma current reaches its final value and the OH coils are crowbarred ($\dot{I}_{OH} = 0$).

In addition to the plasma size and the magnetics information, the input to the plasma-circuit code includes the final values of the plasma and EF-coil currents, the back-bias current for the OH-coil set, the grid voltage, and the value of the transfer resistor (Figure 6.5-1). These latter circuit values determine the evolution of the plasma current during the start-up transients. An analytical estimate of the circuit behavior can be found by ignoring the EF trim-coil and eddy-current circuits and using Equations 6.5-1 through 6.5-3.

Charge-up phase. During the charge-up phase [Figure 6.5-1(A)], the OH coils are charged from the grid. Denoting the back-bias OH-coil current by I_{OH}^- and the duration of the charge-up phase from $-t_{cu}$ to $t = 0$, we have

$$t_{cu} = -\tau_{cu} \ln \left(1 - \frac{I_{OH}^-}{I_{G,CU}} \right), \quad (6.5-18)$$

$$I_{OH}(t) = I_{G,CU} \left[1 - \exp \left(-\frac{t + t_{cu}}{\tau_{cu}} \right) \right], \quad (6.5-19)$$

where $\tau_{cu} \equiv L_{OH}/R_{OH}$, $v_{G,cu}$ is the voltage applied to OH coils during the charge-up phase, and $I_{G,cu} \equiv v_{G,cu}/(N_{OH} R_{OH})$. Using the expression for $I_{OH}(t)$, the maximum power extracted from the grid, $P_{cu,Max}$, is

$$P_{cu,Max} = \frac{v_{G,cu} I_{OH}^-}{N_{OH}} = R_{OH} I_{G,cu} I_{OH}^-. \quad (6.5-20)$$

The total energy extracted from the grid, $W_{G,cu}$, including both the magnetic energy stored in the OH coils ($W_{M,cu}$) and the joule losses during the charge-up phase ($W_{\Omega,cu}$) is

$$W_{G,cu} = I_{G,cu} (v_{G,cu} t_{cu} - L_{OH} I_{OH}^-), \quad (6.5-21)$$

and a measure of the inefficiency of the charge-up phase is

$$\frac{W_{\Omega,cu}}{W_{M,cu}} = -2 \left(\frac{I_{G,cu}}{I_{OH}^-} \right)^2 \ln \left(1 - \frac{I_{OH}^-}{I_{G,cu}} \right) - 1 - \frac{2 I_{G,cu}}{I_{OH}^-}. \quad (6.5-22)$$

Normalized values of t_{cu}/τ_{cu} and $W_{\Omega,cu}/W_{M,cu}$ are presented in Table 6.5-II for different values of $I_{G,cu}/I_{OH}^-$. This table shows that for an efficient charge-up phase (relatively small joule losses in the OH coils), values of $I_{G,cu}/I_{OH}^-$ of 3 or larger is desirable. Smaller values result in large joule losses that should be removed by the OH-coil cooling circuit.

Fast-ramp phase. During both fast- and slow-ramp phases, the OH- and EF-coil circuits are in parallel, that is $v_{OH} = v_{EF}$. The circuit equations (Equations 6.5-1 through 6.5-3) then can be solved by using a perturbation expansion on the small parameter R/L of each circuit. Assuming that the number of turns in OH and EF coils are set according to Equation 6.5-6, the circuit equations can be solved to get

$$\frac{dI_{\phi}}{dt} = -\frac{1}{(C_1 - C_2) L_{OH} N_{OH}} \frac{v_{OH}}{N_{OH}}, \quad (6.5-23)$$

$$I_{OH}(t) = I_{OH}^- - C_1 I_{\phi}(t), \quad (6.5-24)$$

$$I_{EF}(t) = -\left| \frac{I_{EF}^+}{I_{\phi}^+} \right| I_{\phi}(t), \quad (6.5-25)$$

Table 6.5-II.
NORMALIZED PARAMETERS OF THE CHARGE-UP PHASE

Charge-Up Voltage, $I_{G,cu}/I_{OH}^- = v_{G,cu}/(R_{OH} N_{OH} I_{OH}^-)$	Joule Losses, $W_{\Omega,cu}/W_{M,cu}$	Charge-Up Time, $-t_{cu}/\tau_{cu}$ ^(a)
1.01	6.40	4.62
1.1	2.60	2.40
1.2	1.76	1.79
1.5	0.94	1.10
2.0	0.55	0.69
3.0	0.30	0.41
5.0	0.16	0.22
10.0	0.07	0.11

(a) For the TITAN-I design, $\tau_{cu} = 20.7$ s.

and

$$W_M(t) = \frac{1}{2} L_{OH} I_{OH}^{-2} - (C_1 - C_2) L_{OH} I_{\phi}(t) I_{OH}^- + \frac{(C_1 - C_2) L_{OH}}{2 C_4} I_{\phi}^2(t), \quad (6.5-26)$$

where $W_M(t)$ is the total magnetic stored energy in the system (plasma and OH and EF coils), parameters C_1 through C_3 are given by Equations 6.5-7 through 6.5-9, and

$$C_4 \equiv \left(C_1 + \frac{N_{OH}}{N_{EF}} \left| \frac{I_{EF}^+}{I_{\phi}^+} \right| \right)^{-1}. \quad (6.5-27)$$

During the slow-ramp phase, the OH coils are discharged into a transfer resistor, R_{tr} , while the EF coils are connected in parallel to the OH coils [Figure 6.5-1(B)]. Substituting for v_{OH} from

$$v_{OH} = v_{EF} = -R_{tr} \left(\frac{I_{OH}}{N_{OH}} + \frac{I_{EF}}{N_{EF}} \right) \quad (6.5-28)$$

in Equations 6.5-23 through 6.5-25 results in

$$v_{OH}(t) = v_{Max} \exp\left(-\frac{t}{\tau_{fr}}\right), \quad (6.5-29)$$

$$I_{\phi}(t) = C_4 I_{OH}^- \left[1 - \exp\left(-\frac{t}{\tau_{fr}}\right)\right], \quad (6.5-30)$$

and the evolution of OH- and EF-coil currents can be found by substituting for I_{ϕ} from the above equation in Equations 6.5-24 and 6.5-25. Also,

$$\tau_{fr} = \frac{N_{OH}^2 C_4 (C_1 - C_2) L_{OH}}{R_{tr}} \quad (6.5-31)$$

and

$$v_{Max} = \frac{R_{tr} I_{OH}^-}{N_{OH}} \quad (6.5-32)$$

is the maximum voltage that appears on the OH and EF coils. The value of R_{tr} is chosen such that v_{Max} satisfies the electrical-engineering design constraints of the coils.

The fast-ramp phase continues until the voltage across the OH and EF coils becomes equal to the grid power-supply voltage, v_G . The duration of the fast-ramp phase, t_{fr} , is

$$t_{fr} = \tau_{fr} \ln\left(\frac{v_G}{v_{Max}}\right), \quad (6.5-33)$$

and the plasma current at $t = t_{fr}$ is

$$I_{\phi}(t_{fr}) = C_4 I_{OH}^- \left(1 - \frac{v_G}{v_{Max}}\right). \quad (6.5-34)$$

The maximum joule heating in the transfer resistor is at the initiation of the fast-ramp phase ($R_{tr} I_{OH}^{-2}/N_{OH}^2$) and the total joule losses in the transfer resistor, $W_{\Omega, tr}$, are

$$W_{\Omega, tr} = \frac{C_4(C_1 - C_2)}{2} L_{OH} I_{OH}^{-2} \left[1 - \left(\frac{v_G}{v_{Max}}\right)^2\right]. \quad (6.5-35)$$

The joule losses in the OH and EF coils can be found by using the appropriate expressions for the current evolution in each circuit.

Note that larger values of v_{Max} result in larger R_{tr} and shorter duration for the fast-ramp phase. However, the plasma current at the end of the fast ramp, as well as the energy loss in the transfer resistor, is insensitive to the value of v_{Max} since usually $v_G/v_{Max} \ll 1$.

Slow-ramp phase. During the slow-ramp phase, the grid power is directly applied to the OH and EF circuits, driving the OH current to zero and in the forward-bias direction [Figure 6.5-1(C)]. Substituting for $v_{OH} = v_{EF} = -v_G$ in Equations 6.5-23 through 6.5-25 results in

$$I_\phi(t) = I_\phi(t_{fr}) + \frac{v_G}{N_{OH}(C_1 - C_2)L_{OH}} (t - t_{fr}), \quad (6.5-36)$$

and the evolution of OH- and EF-coil currents can be found by substituting for I_ϕ from the above equation in Equations 6.5-24 and 6.5-25. At the end of the slow-ramp phase, t_{sr} , the plasma current has reached its final value. Therefore, the duration of the slow-ramp phase, $t_{sr} - t_{fr}$, is

$$t_{sr} - t_{fr} = \frac{N_{OH}(C_1 - C_2)L_{OH}}{v_G} [I_\phi^+ - I_\phi(t_{fr})]. \quad (6.5-37)$$

The power extracted from the grid, P_G , is given by

$$P_G(t) = \frac{v_G}{C_4 N_{OH}} [I_\phi(t) - C_4 I_{OH}^-]. \quad (6.5-38)$$

The grid voltage, v_G , in the above equations is set based on the constraint of the maximum power extracted from the grid, $P_{G,Max}$, which occurs at the end of slow-ramp phase:

$$v_G = \frac{C_4 N_{OH}}{I_\phi^+ - C_4 I_{OH}^-} P_{G,Max}. \quad (6.5-39)$$

The total energy extracted from the grid during the slow-ramp phase is

$$W_G = \frac{(C_1 - C_2)L_{OH}}{2C_4} [I_\phi^+ - I_\phi(t_{fr})] [I_\phi^+ + I_\phi(t_{fr}) - 2C_4 I_{OH}^-]. \quad (6.5-40)$$

The above equations show that the plasma current and power extracted from the grid increase linearly in time during the slow-ramp phase. At the beginning of this phase, $P_G < 0$ indicates that the OH coils are still discharging into the shunt resistors of the grid power supply, but this part ($P_G < 0$) is of short duration. Also, using Equation 6.5-36, one finds

$$\Delta I_{OH} = I_{OH}^- - I_{OH}^+ = C_1 I_\phi^+, \quad (6.5-41)$$

which shows that parameter C_1 directly reflects the degree of coupling between the OH and plasma circuits.

Equations 6.5-18 through 6.5-41 provide estimates for the evolution of the plasma current during the current ramp-up phase. In addition to the coil geometry and values I_ϕ^+ and I_{EF}^+ , the input data for these equations include the OH-coil back-bias current value, I_{OH}^- , grid voltage for the charge-up phase, $v_{G,cu}$ (or the maximum power extracted from the grid during the charge-up phase, $P_{cu,Max}$), the maximum voltage allowed on the OH and EF coils, v_{max} (or the value of the transfer resistor, R_{tr}), and the maximum power extracted from the grid during the slow-ramp phase, $P_{G,Max}$ (or the grid voltage during the slow-ramp phase, v_G). As mentioned before, the value of the plasma current at the end of the fast-ramp phase is insensitive to the value of v_{max} . A value of $v_{max} = 80$ kV is chosen for the TITAN analysis, which results in a maximum voltage of 40 kV on each superconducting EF coil. It is further assumed that the same power supply is used during the charge-up and slow-ramp phases ($v_{G,cu} = v_G$), and the maximum grid power is set at 500 MW. For these conditions, the solutions to Equations 6.5-18 through 6.5-41 are reported in Table 6.5-III for different values of OH-coil back bias, ranging from $I_{OH}^- = 28$ (symmetric swing for TITAN-I) to 50 MA-turn.

Table 6.5-III shows that as I_{OH}^- is increased, the voltage of the grid power supply also increases and, thus, $I_{G,cu}$ increases such that the ratio of $I_{G,cu}/I_{OH}^-$ asymptotes to about 1.4. As a result, the duration of the charge-up phase asymptotes to ~ 25 s and the ratio of $W_{\Omega,cu}/W_{M,cu}$ to ~ 1 (Table 6.5-II). Since the magnetic stored energy in the OH coil at the end of the charge-up phase increases as I_{OH}^{-2} , joule losses during this phase also increase as the square of the OH back-bias current.

For larger values of I_{OH}^- and for fixed values of v_{Max} , the transfer resistor should be smaller (Equation 6.5-32), resulting in longer τ_{fr} and t_{fr} . The plasma current at the end of the fast-discharge phase is also larger and directly scales with I_{OH}^- . As a result, Equation 6.5-38 shows that for a fixed $P_{G,Max}$, the voltage of the grid power supply is larger, as was mentioned before. Large values of I_{OH}^- , together with the resultant larger values of v_G , increase the plasma-current ramp rate during the slow-ramp phase and decrease the duration of this phase. The OH forward-bias current will also be smaller, such that the total current swing in the OH coils remains the same. The total joule losses in the OH coils during both fast- and slow-ramp phases is approximately constant and independent of I_{OH}^- .

Even though the duration of the current ramp-up phases becomes shorter as I_{OH}^- is increased, τ_{cu} also increases such that the total duration of start-up remains the same. The total energy extracted from the grid increases for larger values of I_{OH}^- , mainly because of increased joule losses in the OH coils during the charge-up phase but also partly because of larger losses in the transfer resistor.

Table 6.5-III.
ESTIMATES OF TITAN-I START-UP PARAMETERS^(a)

Back-bias OH-coil current, I_{OH}^- (MA-turn)	28.	40.	50.
Grid voltage, $v_G = v_{G,cu}$ (kV)	2.50	2.98	3.55
Transfer resistor, R_{tr} (Ω)	1.06	0.74	0.60
Charge-Up Phase			
$I_{G,cu}$ (MA-turn)	50.7	60.5	72.0
Duration, t_{cu} (s)	16.6	22.4	24.5
Maximum power from grid, $P_{G,cu}$ (MW)	188.	321.	478.
Joule losses in OH, $W_{\Omega,cu}$ (MJ)	695.	2030.	3544.
Energy from the grid (MJ)	1770.	4223.	6970.
Magnetic stored energy, $W_M(t=0)$ (MJ)	1075.	2193.	3426.
Fast-Ramp Phase			
τ_{fr} (s)	0.19	0.27	0.33
Duration, t_{fr} (s)	0.65	0.88	1.04
Plasma current, $I_\phi(t_{fr})$ (MA)	4.72	6.70	8.31
OH-coil current, $I_{OH}(t_{fr})$ (MA-turn)	13.1	18.9	23.8
Joule losses in R_{tr} (MJ)	561.	1144.	1787.
Joule losses in OH (MW)	32.4	91.2	172.
Magnetic stored energy, $W_M(t_{fr})$ (MJ)	514.	1049.	1640.
Slow-Ramp Phase			
Rate of increase in I_ϕ (MA/s)	0.82	0.97	1.16
Duration, $t_{sr} - t_{fr}$ (s)	16.0	11.4	8.18
OH-coil current, $I_{OH}(t_{sr})$ (MA-turn)	-28.1	-16.1	-6.09
Joule losses in OH (MJ)	299.	242.	193.
Energy from the grid (MJ) ^(b)	3955.	2780.	1957.
Magnetic stored energy, $W_M(t_{sr})$ (MJ)	4470.	3829.	3597.
Start-Up Total			
Current ramp-up duration, t_{sr} (s)	16.7	12.3	9.2
Total duration, $t_{cu} + t_{sr}$ (s)	33.2	34.6	33.7
Energy from the grid (MJ) ^(b)	6056.	7336.	9292.
Total joule losses in OH (MJ) ^(c)	2101.	2718.	3960.

(a) For $v_{Max} = 80$ kV, $P_{G,Max} = 500$ MW, the TITAN-I magnetics parameters of Table 6.5-I ($C_1 = 3.16$, $C_2 = 0.154$, $C_3 = -5.47$, $C_4 = 0.174$),

$N_{OH} = 372$, $N_{EF} = 156$, single-turn equivalent $R_{OH} = 0.133 \mu\Omega$, and $R_{EF} = 0$.

(b) Does not include joule losses in the plasma during the current ramp-up.

(c) Including joule heating during the transition phase (see text).

As mentioned before, the maximum voltage on the coils, v_{Max} , has only a small effect on the overall start-up scenario since $v_G/v_{Max} \ll 1$ (Equations 6.5-34 and 6.5-35). For example, increasing v_{Max} from 80 to 100 keV for the case of $I_{OH}^- = 40$ MA-turn of Table 6.5-III reduces t_{fr} to 0.75 s but has negligible effect on any other parameter.

Analysis of Table 6.5-III shows that the start-up scenario strongly depends on the values of I_{OH}^- and $P_{G,Max}$. For a steady-state reactor where start-up is an infrequent event, the total energy absorbed from the grid is not an issue and the cost of the start-up power supply is directly proportional to its capacity, $P_{G,Max}$. The OH-coil back-bias value, on the other hand, has important implications for the design and cost of the OH-coil system. Equation 6.5-41 and values from Table 6.5-III show that for a fixed final plasma current and coil geometry, the current swing in the OH coil, ΔI_{OH} , is constant (56 MA-turn for TITAN-I). Therefore, a symmetric swing $I_{OH}^- = 28$ MA-turn results in smallest peak stresses in the coils.

It is preferable for the OH-coil cooling circuit to only be designed to handle the steady-state heat generated in these coils by nuclear heating and by the oscillating-field current-drive (OFCD) system. For the TITAN-I design, the steady-state heat generation in the OH coils is about 14 MW (Section 10.5.1.1), which is much lower than the heat generated during start-up. The start-up joule losses are absorbed by the thermal inertia of the coils, adiabatically raising the temperature of the conductor. Larger start-up joule losses are associated with larger values of I_{OH}^- . On the other hand, smaller values of I_{OH}^- result in larger values of I_{OH}^+ and larger joule losses during the transition phase to steady state [Figure 6.5-1(D)] where the OH coils are discharged very slowly (L/R time). Since the smallest resistance possible is for short-circuited OH coils, the longest transition time is the same as τ_{cu} (21 s for TITAN-I). For this case, the magnet energy stored in the forward-biased OH coil appears as heat in the OH coils. The total OH joule losses for the start-up, listed in Table 6.5-III is based on this assumption and shows that the heat deposited in the OH coils scales roughly as I_{OH}^- (and not the square of the current).

The magnet engineering constraints point towards a symmetric OH current swing as the preferred mode of operation. However, it should be noted that during the transition phase, the current-drive system should work harder to oppose the electric field generated in the plasma by the discharging OH coils. Since the maximum decay time of the OH circuit is set by t_{cu} and is independent of I_{OH}^- , smaller values of back bias (larger I_{OH}^+) will require higher excess capacity for the OFCD system. Finally, lower values of I_{OH}^- increase the duration of the slow-ramp phase such that the amount of energy supplied to the plasma during this phase may not be enough to balance the transport losses. In fact, for TITAN-I start-up simulations, ignition could only be achieved for $I_{OH}^- = 50$ MA-turn

as is discussed below. This is partly caused by the assumption of a constant-voltage, v_G , power supply for the grid. This assumption causes grid power used by the system to increase linearly in time (Equation 6.5-38), and the full capacity of the power supply is utilized only for a small portion of the start-up sequence. In principle, one can envision a scenario in which a large voltage is applied at the beginning of the slow-ramp phase (larger plasma-current ramp rate) and then slowly reduced, step by step, such that large power can be extracted from the grid at all times. This procedure reduces the duration of the slow-ramp phase by up to 50% and will allow for symmetric OH-coil current swings.

The above discussion shows that the optimum value of I_{OH}^- can only be obtained through complex analyses of the detailed OH-coil design, the OFCD-system excess-capacity requirements, and the extra cost that may be associated with a variable-voltage grid power supply. Because of the complexity of this optimization problem, and because the cost of the OH system and the start-up equipment represents a very small fraction of the cost of the TITAN reactors, such an optimization was not performed.

The plasma-circuit analysis of the TITAN-I design uses $I_{OH}^- = 50$ MA-turn and other relevant parameters that are similar to those listed in the footnote of Table 6.5-III. Figures 6.5-4 through 6.5-9 show the evolution of the TITAN-I plasma during the start-up sequence, ignoring the eddy currents that may be flowing in the FPC. Figure 6.5-4 shows the time histories of the plasma and PF circuit currents. Because of the effect of plasma resistance, the EF-coil current reaches its final value before the plasma current and is crowbarred first. These figures also show the required current for the EF trim coil to achieve the exact equilibrium throughout the discharge. The vertical field provided by the main EF is shown in Figure 6.5-5(A) and is compared to the required value from the Shafranov formula (Equation 6.5-11). The vertical field provided by the EF trim coil to produce the exact equilibrium is also shown. The value of N_{OH}/N_{EF} is slightly adjusted, as compared to the value from Equation 6.5-6(A), to minimize the power to the EF trim circuit. The values of currents and the duration of the the discharge are comparable to the estimates of Table 6.5-III.

Figure 6.5-5(B) shows that total power extracted from the grid and the power delivered to the OH and EF coils during the start-up sequence. which, again, are in good agreement with the analytical estimates. At $t \simeq 11$ s, final EF-coil current is achieved and the EF coils are crowbarred resulting in a drop in EF-coil power (and grid power). Since the plasma and OH-coil currents are still changing, power has to be supplied to the EF-coil in order to maintain the EF-coil current. Full plasma current is achieved at $t \simeq 13$ s and OH coils are crowbarred, resulting in decreases in OH- and EF-coil powers. Between $t \simeq 13$ and 15 s, β_θ and, therefore, plasma inductance, are changing rapidly.

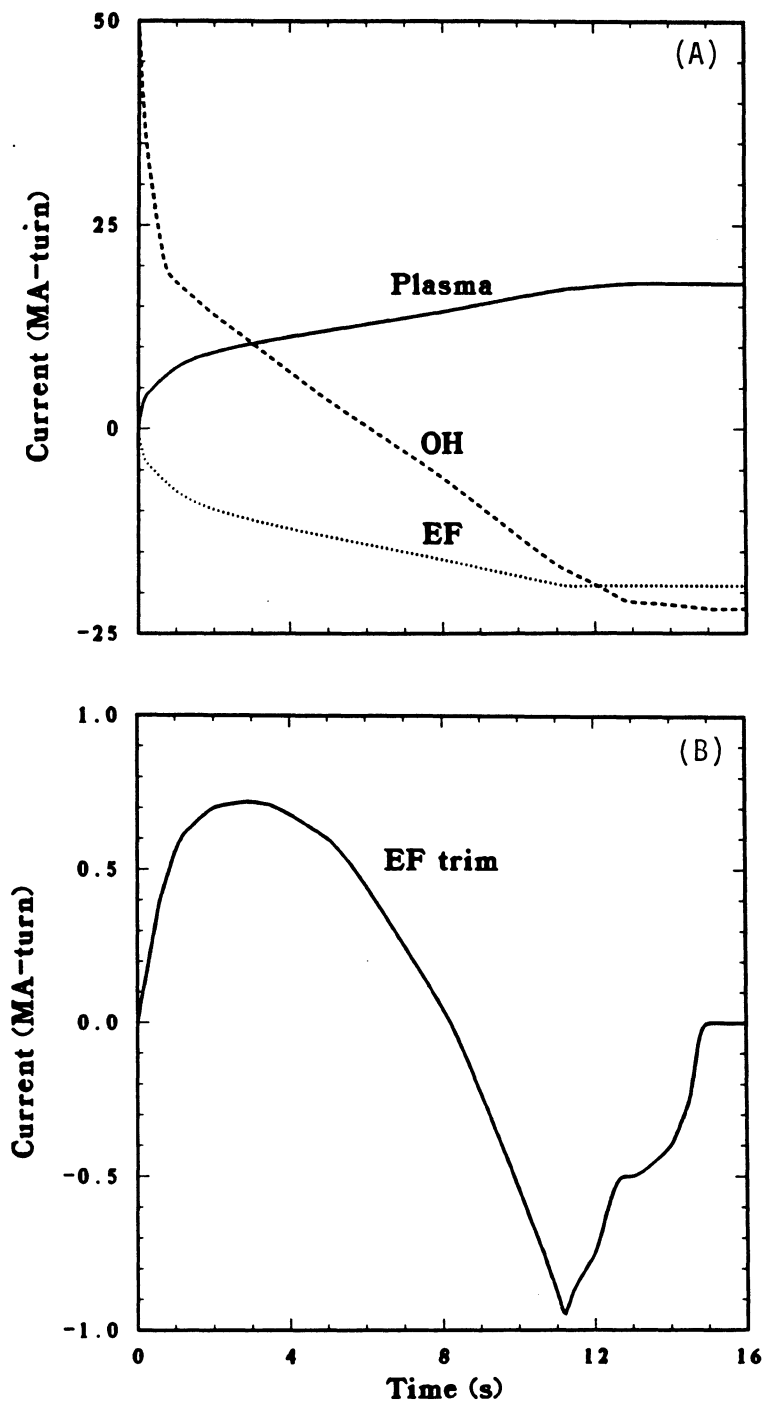


Figure 6.5-4. The TITAN-I start-up simulation results for the evolution of the current in (A) the plasma, superconducting EF coil, and OH coil; and (B) the EF trim coil.

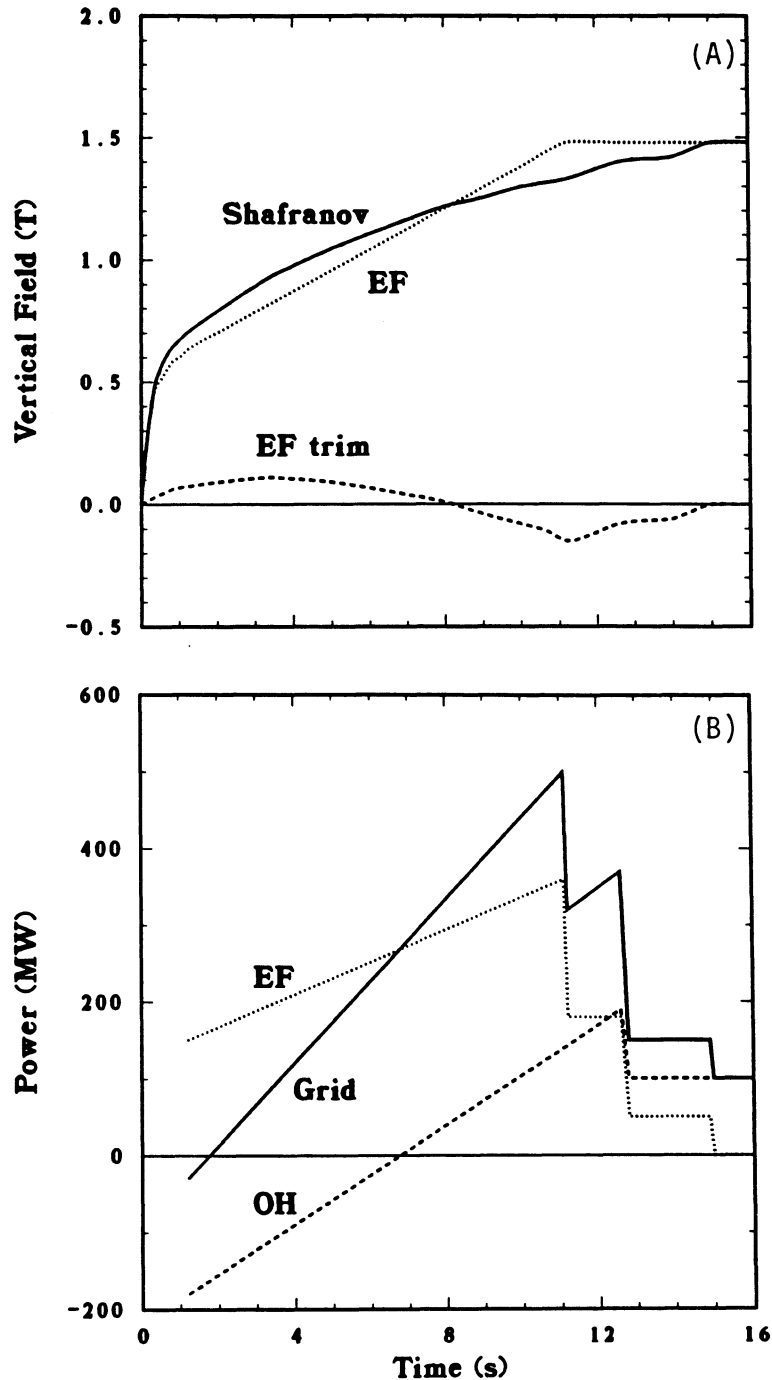


Figure 6.5-5. The TITAN-I start-up simulation results for the evolution of (A) vertical fields produced by the superconducting EF and EF trim coils and the required vertical field from the Shafranov formula; and (B) power deposited in the superconducting EF coil, OH coil, and the total power extracted from the grid.

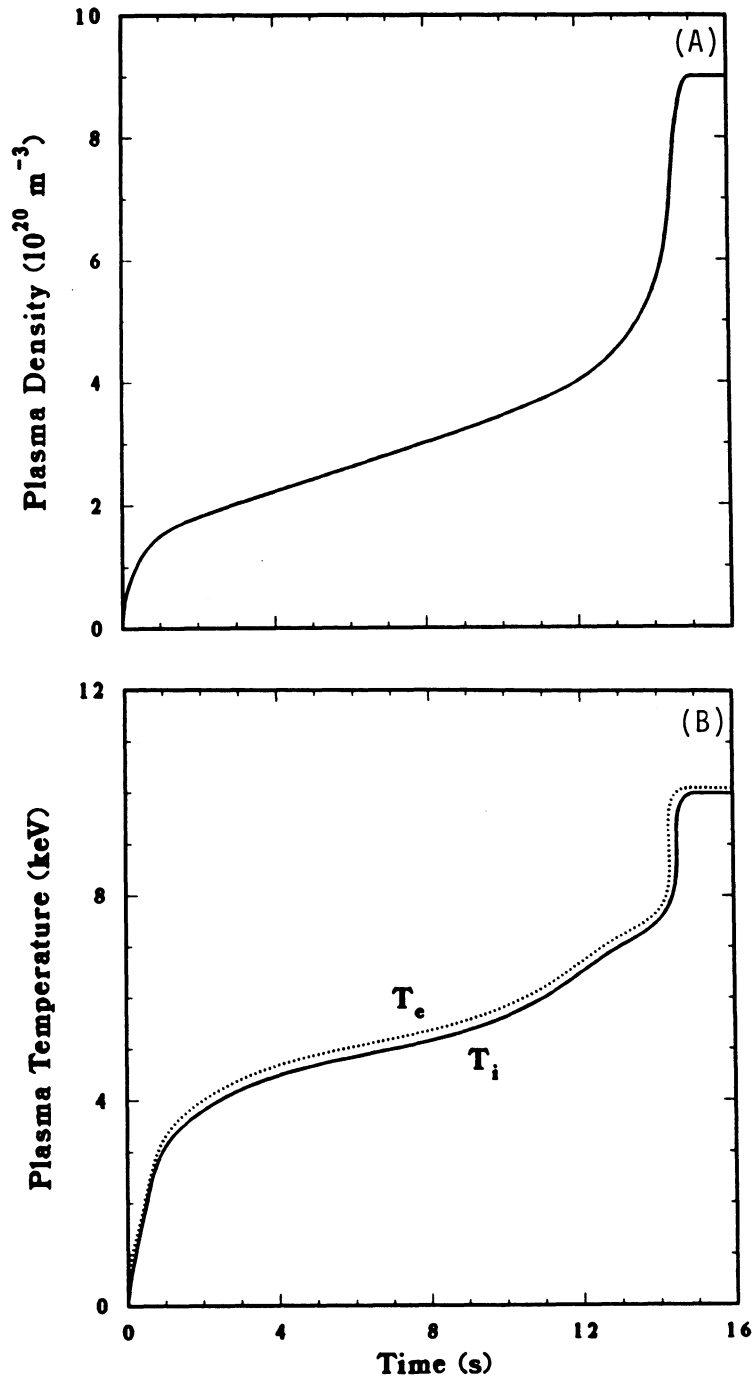


Figure 6.5-6. The TITAN-I start-up simulation results for the evolution of plasma density (A) and temperature (B).

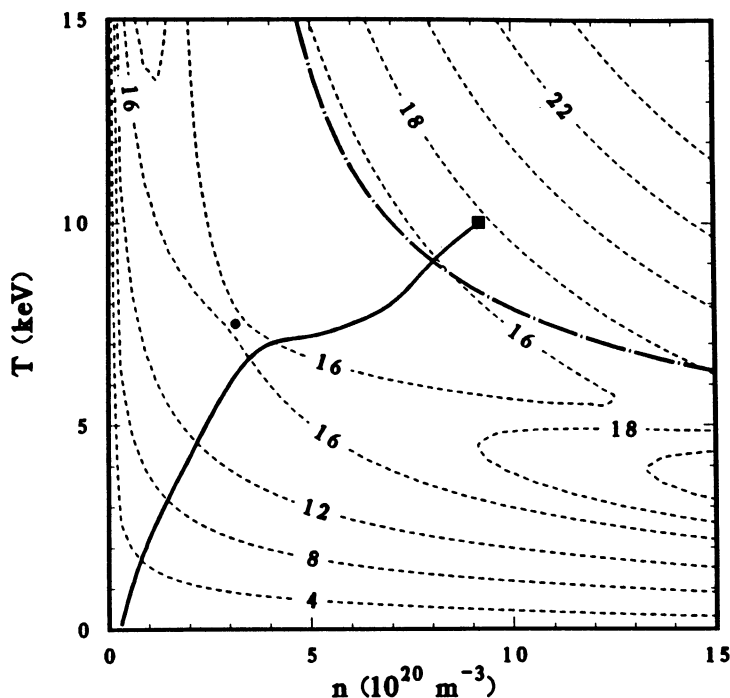


Figure 6.5-7. The TITAN-I start-up path projected in the I_ϕ - n - T space as found by the analysis of the ignition requirements (Figure 6.4-1). The start-up path (solid line) passes close to the saddle point.

During this period, the trim-coil current is also dropping to zero. Some power still has to be applied to the EF-coil to counter the two effects. The OH-coil power after $t \simeq 13$ s is mostly due to joule heating in the OH coils. It should be noted that the current, voltage, and power to the EF trim-coil circuit is calculated to keep the plasma in exact equilibrium (no shift in magnetic axis). Permitting small shifts in the plasma position will greatly reduce the power required for the EF trim circuit.

Figure 6.5-6 shows the evolution of plasma density and temperature during the start-up sequence. The evolution of plasma density and temperature in the ignition I_ϕ - n - T space is shown in Figure 6.5-7. The ion density evolution is an input to the plasma-circuit code and was adjusted to ensure that the start-up path is located close to the ignition saddle point. The corresponding fueling rate is calculated from the particle balance equation and is shown in Figure 6.5-8(A). The evolution of the plasma density is also chosen such that the plasma streaming parameter remains small and the electron runaway condition is avoided [Figure 6.5-8(B)]. The evolution of β_θ and the volt-second

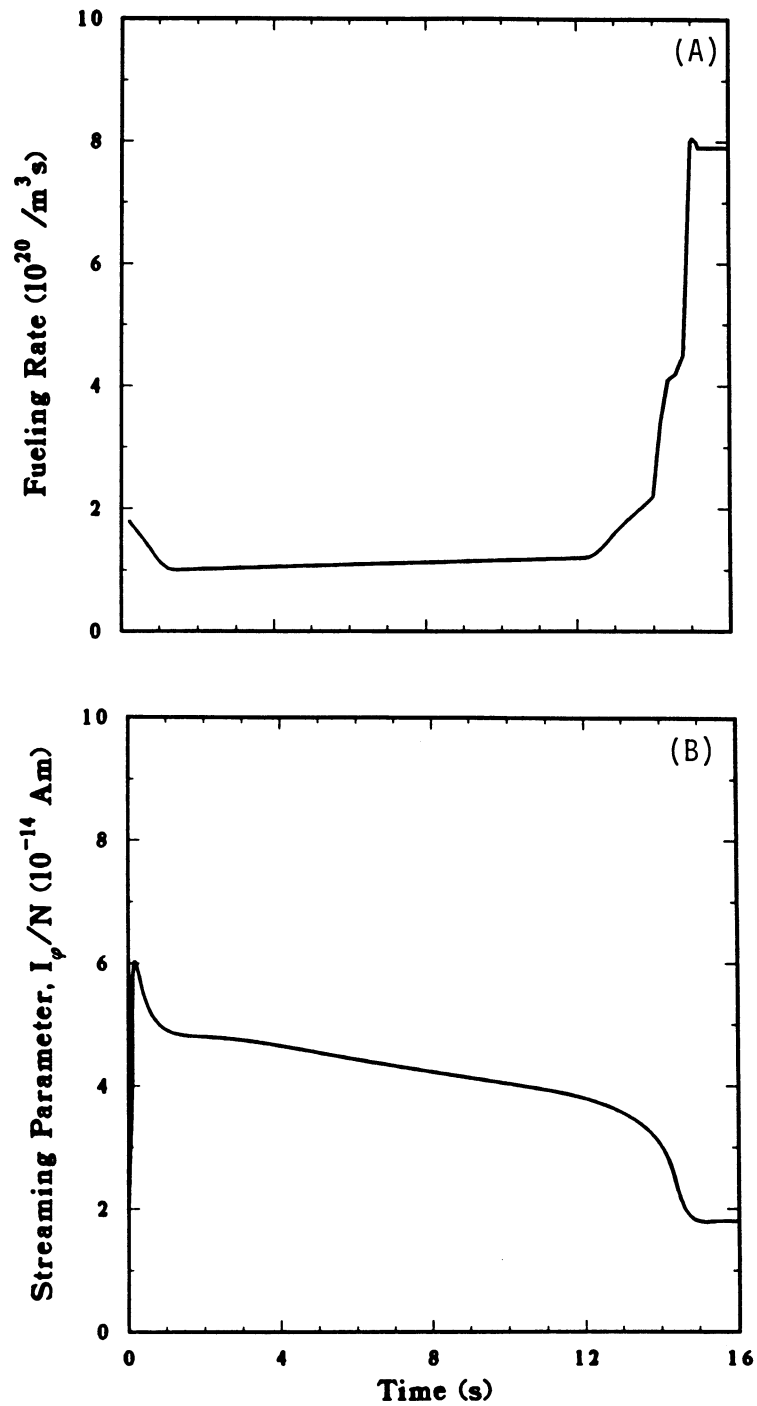


Figure 6.5-8. The TITAN-I start-up simulation results for the required fueling rate (A) and the resultant plasma streaming parameters, I_ϕ/N (B).

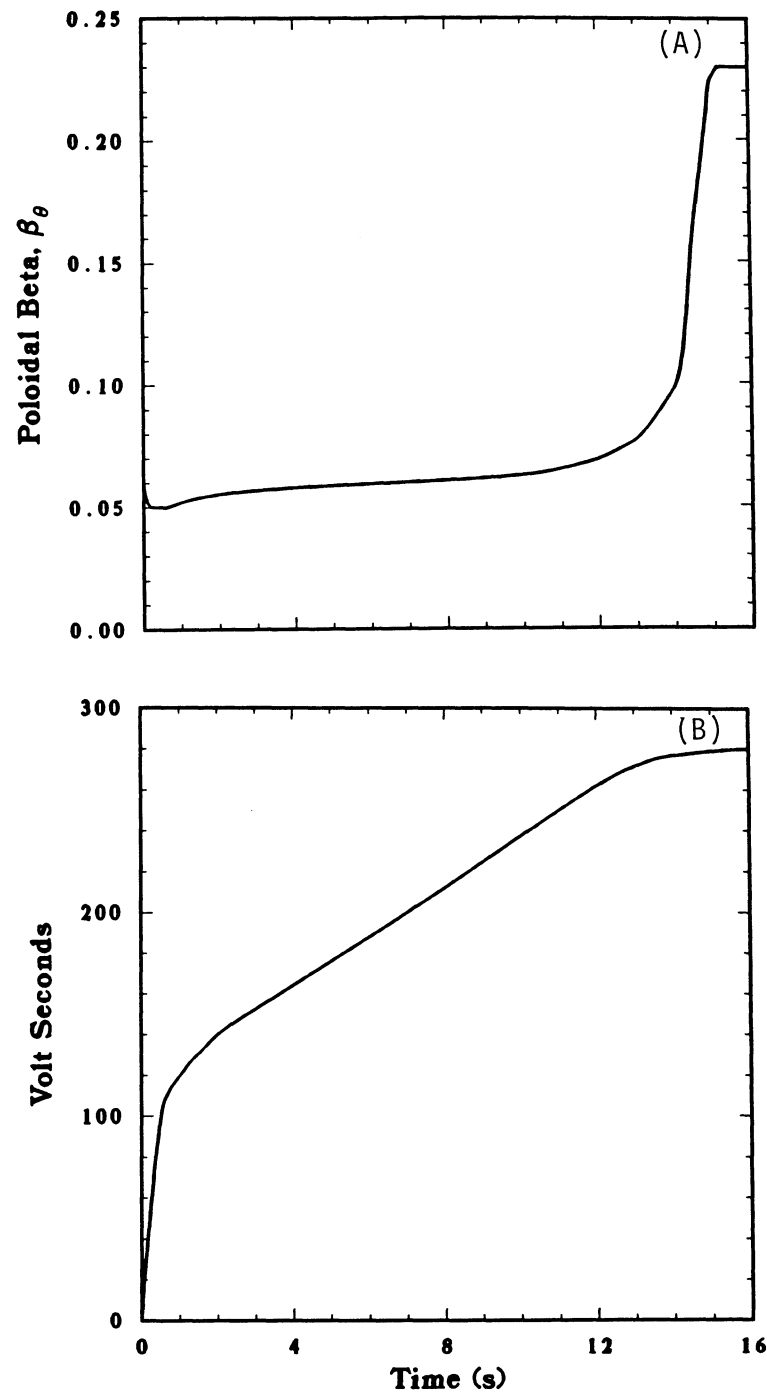


Figure 6.5-9. The TITAN-I start-up simulation results for the evolution of β_θ (A) and the consumed volt-seconds (B).

consumption during the start-up sequence are shown in Figure 6.5-9. It can be seen that plasma ignition is achieved at β_θ values of about 8% and that the final value of β_θ is achieved only after ignition.

The impact of the eddy currents on the start-up sequence has also been studied. The TITAN-I FPC is located in a thick vacuum tank with no resistive break. However, resistive breaks are used in the FPC itself. As a result, the eddy currents in the tanks produce the dominant effect on the start-up. Because the magnitudes of the eddy currents are small, the evolution of the plasma current is not affected. The vertical fields produced by the eddy currents, even though small, affect the plasma equilibrium during the fast-discharge phase (Figure 6.5-10) and programming voltage to the EF trim coils should be modified to keep the plasma in exact equilibrium. However, the power requirement for the EF trim power supplies is not increased by the presence of eddy currents.

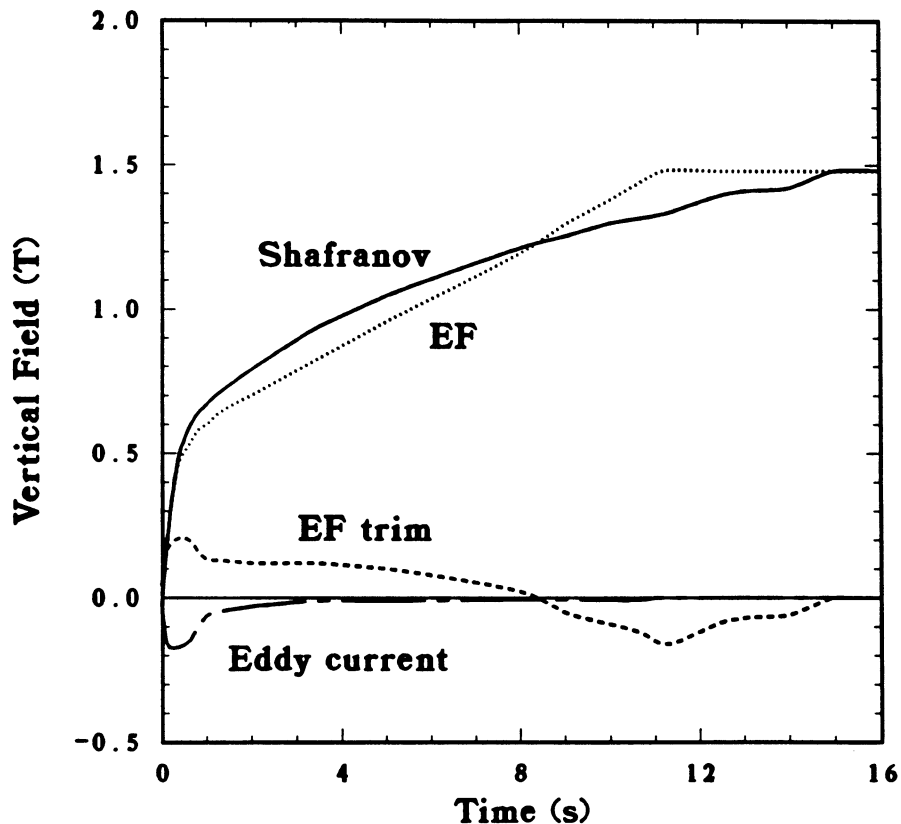


Figure 6.5-10. The TITAN-I start-up simulation results for the evolution of vertical fields produced by the superconducting EF-coil, EF-trim coil, and eddy currents, and the required vertical field from the Shafranov formula.

6.6. SHUTDOWN & TERMINATION OF TITAN PLASMA

In RFPs and tokamaks, in addition to the plasma thermal energy, a significant amount of energy is stored in the poloidal magnetic field. At full operational conditions, the stored energy in TITAN-I plasma includes 0.1 GJ of kinetic (thermal) energy and $W_M \sim 4.3$ GJ of magnetic energy (~ 5.2 GJ for OH coils with full forward-bias current). The magnetic energies internal to the plasma are 0.3 MJ in the toroidal field and 0.4 GJ in the poloidal field. The magnetic energies outside the plasma are < 2 MJ in the toroidal field and 3.6 GJ in the poloidal field. Any rapid release of these stored energies (*e.g.*, similar to disruptions in tokamaks) may lead to severe consequences.

Operating RFP experiments usually end with a "current termination" phase where the plasma current is rapidly reduced to approximately zero. Current termination is characterized by the loss of toroidal-field reversal and is accompanied by a positive voltage spike (as opposed to a negative voltage spike for tokamak disruptions) and large density and magnetic-field fluctuations. A number of variables, such as plasma density, toroidal-field reversal, magnetic-field errors, and impurities appear to affect RFP terminations. A complete and satisfactory explanation of RFP current terminations is not yet available. Evidence, however, suggests that the onset of termination may be related to a loss of density, possibly leading to a streaming parameter that exceeds a critical value for runaway electrons. Since the value of the streaming parameter for the TITAN plasma is only a percent of the critical value for runaway electrons, a current termination is not expected during normal, steady-state operation of the TITAN reactor; rather only failure of plasma support technologies leading to an uncontrolled ramp-down of the plasma current will result in a current termination.

A method of controlled current ramp-down has been tested on the HBTX1B experiment in which the TF-coil circuit is controlled so that the pinch parameter (and the field reversal) is maintained at a given value as the current is decreased to a relatively low level [2]. Maintaining the field reversal in this way is found to delay termination, and the current can be reduced to between 10% and 20% of the maximum value (and the stored magnetic field energy reduced to 1% to 4% of the maximum value) before the termination occurs. Controlled ramp-downs of this kind forestall the loss of toroidal-field reversal as long as possible and are required for the reactor.

6.6.1. Plasma Accidents

During normal, steady-state operation of the TITAN reactors, the following plasma support technologies are operational: (1) fueling, (2) current-drive, (3) toroidal-field, (4) divertor-field, and (5) equilibrium-field systems. Consequences of failure of each of these systems are discussed below.

Fueling system. The effective particle-confinement time in the TITAN plasma is very long (a few seconds) because of the operation with high-recycling divertors. The standard shutdown scenario envisioned for the TITAN plasma starts with the termination of plasma fueling and current divertor operations. Therefore, the loss of fueling system (and vacuum pumping) will not initiate an accident and the standard plasma shutdown scenario will be implemented.

Current-drive system. Once the current drive fails, the plasma current will resistively decay with time scales of $L_p/R_p \simeq 200$ to 400 s. As for the case of failure of the fueling system, the standard plasma shutdown scenario can be implemented here which will prevent any accidents.

Toroidal-field system. The TF coils provide the reversed toroidal field at the plasma edge. If the TF-coil system (power supplies) fail, the RFP dynamo activity would increase to generate the necessary toroidal flux, resulting in a decay of the plasma current. An emergency plasma shutdown is recommended in this case even though the decay time for the plasma current is probably long enough that a standard shutdown would be possible.

Divertor-field system. The TITAN reactors operate with three toroidal-field divertors. If any of the divertor coils fail, the reactor can still be operated at reduced power levels. Failure of all three divertors will result in the plasma "riding" on the first wall in a limiter mode. Since the first wall is designed to handle about 95% of the plasma heat flux (if distributed uniformly on the first wall), a standard shutdown process would probably suffice to avert any accidents.

Equilibrium-field system. The TITAN reactors use two sets of EF coils: a pair of superconducting magnets provide the main equilibrium field, and a pair of small normal-conducting "trim" coils provide the exact equilibrium (for feedback control of plasma

position and for OFCD cycles). With a loss of control on plasma equilibrium and position, not only can the plasma energy be deposited locally, but also the plasma current will decrease rapidly, usually leading to a disruption or current termination. The failure of the equilibrium-field system, therefore, appears to be the most severe plasma-related accident for the TITAN reactor (and for any current-carrying toroidal system).

6.6.2. Shutdown Procedures

The TITAN plasma shutdown procedures are guided by the above observations to ensure (1) plasma current is reduced through a controlled ramp-down in order to forestall current termination, (2) plasma equilibrium is maintained during current ramp-down, (3) failure of the equilibrium-field system (*i.e.*, quench of the superconducting EF coils) will automatically lead to an emergency shutdown, and (4) most of the magnetic energy stored in the plasma is removed during the shutdown.

The plasma shutdown scenarios envisioned for the TITAN plasma, therefore, start with terminating fueling and current-drive operations and simultaneously discharging the EF coils. For the standard shutdown procedure, the duration of the EF-coil discharge can be on the order of a few to tens of seconds. During the emergency shutdown procedure, however, the EF coils are discharged rapidly (~ 0.1 s) through a resistor that can be combined with the quench protection system for the EF coils. Therefore, failure of the equilibrium-field system will automatically initiate the emergency shutdown procedure.

Because of the strong magnetic coupling between the plasma and EF and OH coils in TITAN, a fast discharge of the EF coils results in a rapid decrease in the plasma current; that is, the plasma stored magnetic energy is removed through the EF-coil circuit rather than appearing as heat on the first wall. The parameters of the EF- and OH-coil circuits, however, are chosen such that the plasma equilibrium is approximately maintained during this discharge without any need for an equilibrium control system. The large time constant of the IBC TF coils for field penetration is also utilized to ensure maintenance of the field reversal during the shutdown in a manner similar to the controlled current ramp-down [2].

6.6.3. Termination Simulations

A series of simulations with the plasma-circuit code has been performed to assess the effects of plasma termination and the effectiveness of the above procedures in reducing

the impact of termination. In these simulations, full plasma parameters are assumed at time $t = 0$. The effect of current termination is simulated by an exponential increase in the value of the plasma resistance:

$$R_p(t) = R_p(0) \exp\left(\frac{t}{\tau_{MHD}}\right), \quad (6.6-1)$$

where τ_{MHD} is the growth time of resistive MHD modes perceived to be responsible for loss of reversal and termination (~ 10 ms for TITAN) and $R_p(0)$ is the classical plasma resistance at time t which is computed based on plasma temperature at that time.

The first case simulates the situation where the EF coils remain at full current. The evolution of the plasma current is shown in Figure 6.6-1(A). Because the plasma resistance is very small at time $t = 0$, the plasma current starts to decrease at about 80 ms and is reduced to zero in about 30 ms. Figure 6.6-1(B) shows the joule heating in the plasma, which is assumed to be directly deposited on the first wall. The ~ 4 -GJ magnetic stored energy in the plasma appears as heat at a peak rate of ~ 120 GW. If the OH coils are short-circuited during normal operation, a large current can be induced in the OH coils, reducing the heat deposited in the plasma to ~ 1.6 GJ and the peak heating to ~ 60 GW. The loop voltage induced in the plasma is ~ 20 kV and large voltages also appear on superconducting EF coils. These results underline the severity of the problem.

For the second case, it is assumed that at the initiation of the accident the superconducting EF coils discharge rapidly in a resistor that can be combined with the quench protection system for the EF coils. It is further assumed that OH coils are shorted out. The evolution of circuit currents and the corresponding heating power in the plasma are shown in Figure 6.6-2. It can be seen that the major part of the magnetic stored energy in the system is removed through the discharge of the EF coils. The total energy that appears as heat in the plasma (and, therefore, on the first wall) is ~ 400 MJ, representing a factor of 10 reduction. The peak heating rate and the plasma loop voltage are also reduced tenfold. Because the TITAN PF-coil system is designed to provide approximate equilibrium during the start-up phase, approximate equilibrium is also maintained during the fast discharge of the EF coils as shown in Figure 6.6-3. The change in the plasma position, because of the mismatch between the vertical field and the required field from Shafranov formula, is small during most of the termination simulation. The eddy-current effects have also been investigated and, although small, found to improve the situation (*i.e.*, smaller energy appears in the plasma and less mismatch occurs between the required vertical field and that produced by the EF coils).

These preliminary simulations of the TITAN emergency shutdown procedure appear to indicate that most of the stored magnetic energy is removed from the system and

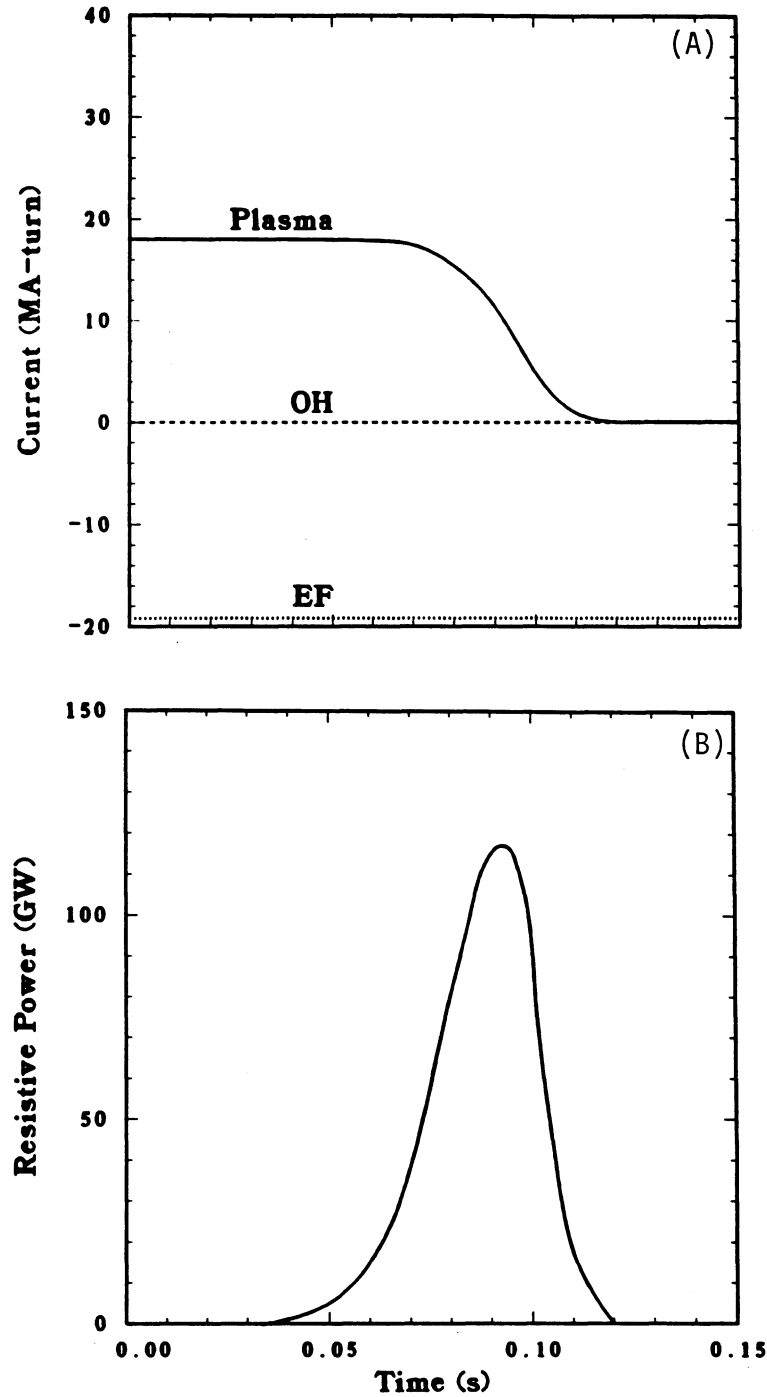


Figure 6.6-1. The TITAN-I termination simulation results for the evolution of (A) the plasma, EF-coil, and OH-coil currents; and (B) the heating power in the plasma. Note that the EF-coil current is kept at its full value and the OH-coil is open circuit.

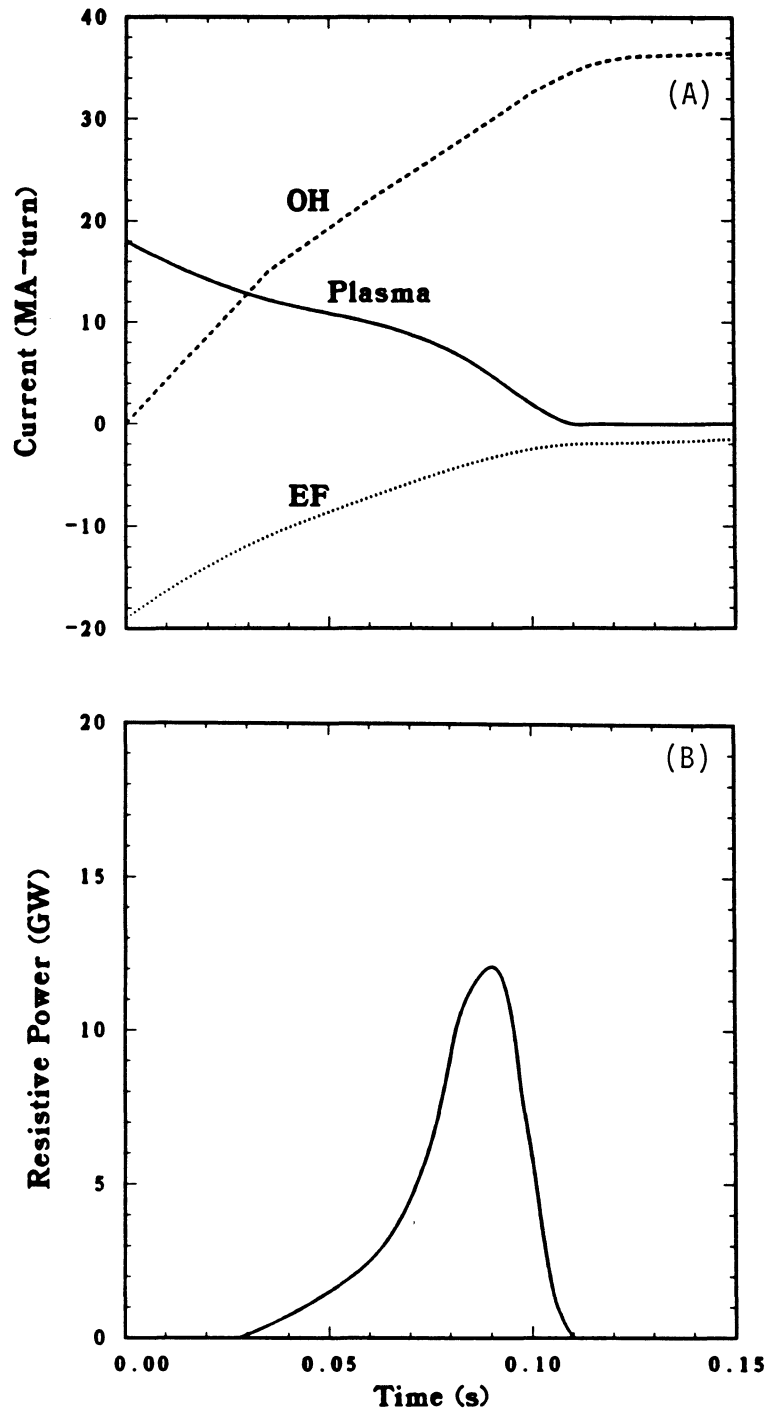


Figure 6.6-2. The TITAN-I termination simulation results for the evolution of (A) the plasma, EF-coil, and OH-coil currents; and (B) the heating power in the plasma. Note that heating power is reduced tenfold in this case.

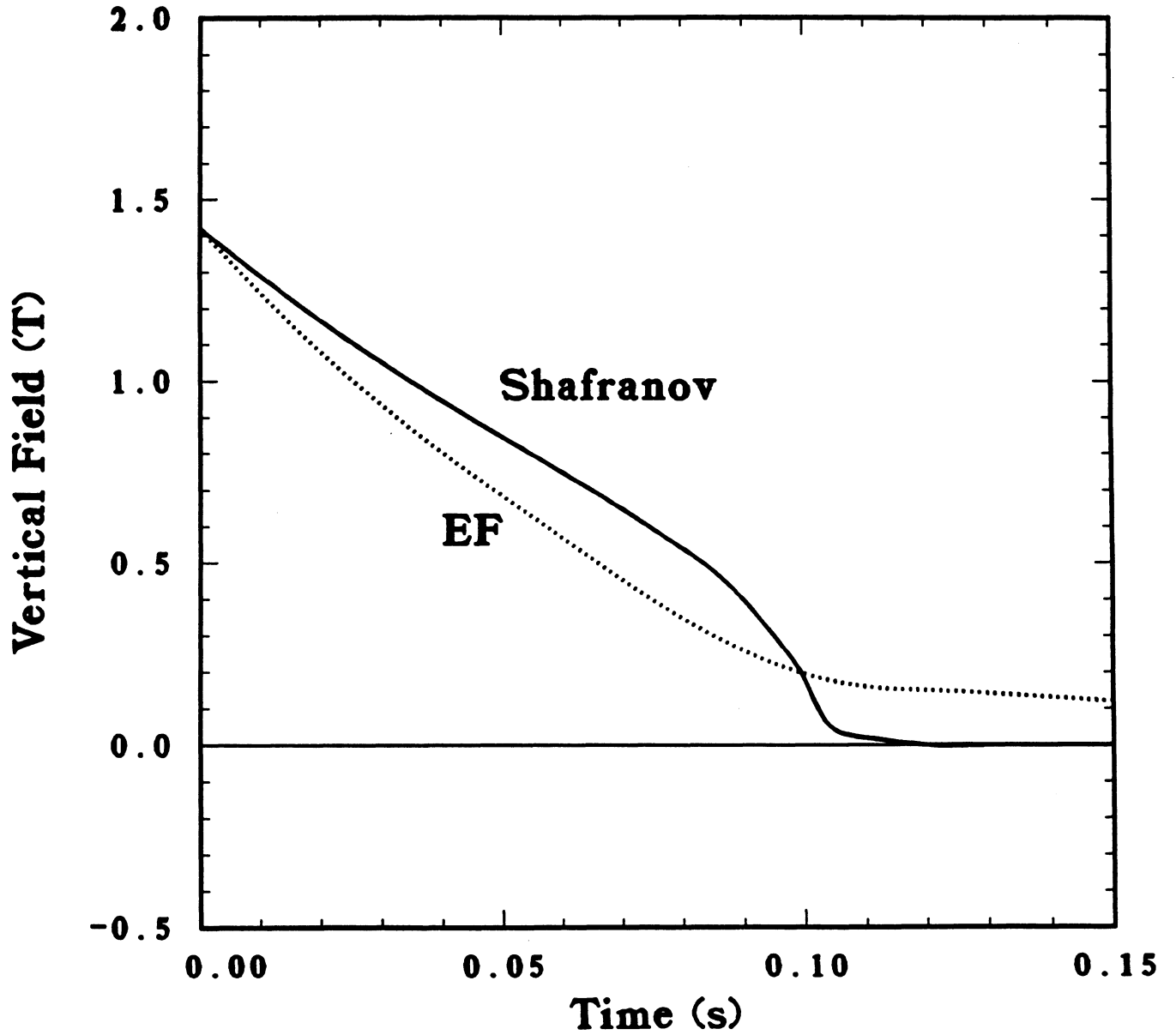


Figure 6.6-3. The TITAN-I termination simulation results for the evolution of vertical fields produced by the superconducting EF-coil current and the required vertical field from the Shafranov formula.

dumped through the discharge resistor. Only about 200 MJ of energy is transferred to the first wall in a time scale of 50 to 100 ms, resulting in an average temperature rise in the first wall of about 300 °C; therefore, failure of the first wall is not expected.

Despite these favorable results, the RFP theoretical and experimental data base is not very extensive. In particular, no experimental data on high-current, high-temperature, diverted RFP plasmas exist. Furthermore, a complete and satisfactory explanation of current termination in RFPs is not yet available. The safety impact of plasma accidents, therefore, should be further investigated and the shutdown procedures, such as those envisioned for the TITAN plasma, should be experimentally explored.

6.7. SUMMARY AND CONCLUSIONS

A typical reversed-field-pinch (RFP) experimental discharge can be divided into four phases: (1) breakdown and formation, (2) current ramp-up, (3) sustainment, and (4) termination. Ignition and fusion burn in a reactor are achieved during the current ramp-up phase, and operation of the current-drive system is required during the sustainment phase. The breakdown and formation phase encompasses the time from the start, which begins by establishing a toroidal magnetic field inside the discharge chamber in the absence of the plasma, to the formation of a "seed" RFP plasma. At the time of peak toroidal magnetic field, poloidal-field windings are activated to produce a flux change through the center of the torus and, consequently, a toroidal voltage around the discharge chamber. This voltage typically ionizes the gas in a few microseconds and the toroidal current is initiated in the resulting plasma. The toroidal plasma current and the toroidal magnetic field within the plasma increase while the toroidal magnetic field at the wall decreases, keeping the average toroidal field (and the toroidal flux) in the chamber almost constant. Eventually the toroidal magnetic field at the wall changes sign and is crowbarred in the reverse direction relative to the back-biased condition of the breakdown and formation phase.

The existing RFP experimental data base for RFP formation and start-up was reviewed in Section 6.2 and was then applied to the TITAN designs (Section 6.3). To summarize, the conditions for plasma breakdown and subsequent RFP formation for the reactor are expected to differ little from the conditions in present and planned RFP experiments [13]. Likewise, the conditions of the seed RFP plasma required to start up the TITAN reactor, except for plasma size, are similar to present-day RFP parameters ($I_\phi = 0.2$ to 0.4 MA, $n = 1$ to $3 \times 10^{19} \text{ m}^{-3}$, $T = 0.1$ to 0.4 eV). For the reference

formation scenario, loop voltage in the range of 200 to 500 V is necessary to ensure short formation time and acceptable resistive flux consumption and formation energy. The scaling of plasma resistivity during the formation phase is an important issue that may be resolved with data from larger RFP experiments. Better density and impurity control during the breakdown and formation process may also be required.

Formation of a seed RFP with somewhat smaller $j_{\phi o}$ (and lower $B_{\phi o}$ and n but higher $\beta_{\theta o}$) would reduce the formation time and is desirable (but requires the relaxation of the $j_{\phi o} = 0.4 \text{ MA/m}^2$ connection to ZT-40M). For example, $j_{\phi o} = 0.28 \text{ MA/m}^2$ and $n_o \simeq n = 2.8 \times 10^{19} \text{ m}^{-3}$ ($j_{\phi}/n = 10^{-14} \text{ A m}$) result in $\xi = 0.011$ and $\beta_{\theta o} = 0.2$ for $T_e = 100 \text{ eV}$. This 30% reduction in $j_{\phi o}$ results in reductions of 30% in τ_R , 40% in resistive flux consumption, and 60% in resistive formation energy for the same value of $E_{\phi o}$. For this case, however, the initial bias field is $B_{\phi o} = \langle B_{\phi} \rangle = 70 \text{ mT}$, which satisfies the stray vertical-field constraint for TITAN-I but violates this constraint for TITAN-II.

Using these seed RFP conditions, a 0-D, profile-averaged plasma-circuit code is used to simulate the evolution of the TITAN plasma through current ramp, ignition, and burn transients (Section 6.5). During the current ramp phase, the plasma current is increased to the peak value. The poloidal-field (PF) coil system provides the poloidal flux and the majority of toroidal flux contained within the full-current plasma by the RFP dynamo.

The steady-state analysis of global plasma power balance provides useful information for the optimization of the plasma approach to ignition. Results of this type of analysis for auxiliary-heated fusion devices are usually presented in the form of required auxiliary power for power balance as a function of plasma density and temperature. This information is then used to identify the path to ignition that requires minimum auxiliary-heating power. A similar analysis can be applied to compact RFP reactors in which the plasma is heated to ignition by ohmic heating alone (no auxiliary heating). The ignition requirements for ohmically heated RFPs are studied (Section 6.4) in order to identify the optimum path for TITAN start-up. It was shown that the results of this analysis can be presented as the required current for power balance as a function of plasma density and temperature. Also, the resultant surface includes a "ridge" in the I_{ϕ} - n - T space above which the path to ignition and burn should be located (similar to corresponding diagrams for auxiliary-heated devices where a ridge for auxiliary heating exists). The optimum ignition scenario attempts to pass over the ridge at its lowest height (saddle point). This saddle point for TITAN designs is located at $T \simeq 7 \text{ keV}$ and $n \simeq 3 \times 10^{20} \text{ m}^{-3}$ with a current of $I_{\phi} \simeq 16 \text{ MA}$. The TITAN start-up path through ignition and burn passes close to this saddle point (Section 6.5.3).

The TITAN start-up scenario through current ramp, ignition, and burn transients is chosen such that the start-up power is directly extracted from the power grid without requiring an on-site power-storage system. This start-up scenario is described in Section 6.5.1 and its implications for the PF-coil system are reviewed. The evolution of the TITAN plasma during the start-up sequence is investigated by using a 0-D, profile-averaged plasma-circuit code. The simulation results are presented in Section 6.5.3. Analytical estimates of the start-up sequence were also produced which agree well with simulation results. To summarize, the full plasma parameters can be achieved in < 12 s by utilizing grid power supplies; no on-site storage facility is necessary. The TITAN PF coils are designed such that the superconducting EF coils provide an approximate equilibrium during the start-up sequence and a pair of small, normal-conducting EF trim coils maintain the exact equilibrium. Using this approach, only the power supplies for the EF trim coils have to be feedback controlled to ensure proper equilibrium.

Reversed-field-pinch discharges normally end abruptly and the plasma current decreases rapidly to zero. Accompanying this fast current "termination" is a positive pulse in the toroidal voltage at the liner. This current termination is in contrast to the negative spike in toroidal voltage that accompanies the current disruption in a tokamak, indicating a difference in the flow of magnetic energy to or from the plasma during the respective events. Furthermore, the RFP current termination can be influenced through the control of the density or toroidal magnetic field [2]; generally, the RFP terminates only when toroidal-field reversal is lost.

Current termination is a safety and economic concern because of large magnetic stored energy in the TITAN plasma. Techniques for control of current termination and plasma shutdown, leading to a "soft-landing," are discussed in Section 6.6. The preliminary simulations of the TITAN emergency shutdown procedure appear to indicate that by discharging the superconducting EF coils at the initiation of the accident, most (90%) of the stored magnetic energy is removed from the system and dumped through the discharge resistor. Only about 200 MJ of energy is transferred to the first wall in a time scale of 50 to 100 ms, resulting in an average temperature rise in the first wall of about 300 °C; therefore, failure of the first wall is not expected.

Despite these favorable results, the RFP theoretical and experimental data base is not very extensive. In particular, no experimental data on high-current, high-temperature, diverted RFP plasmas exist. Furthermore, a complete and satisfactory explanation of current termination in RFPs is not yet available. The safety impact of plasma accidents, therefore, should be further investigated and the shutdown procedures, such as those envisioned for the TITAN plasma, should be explored experimentally.

REFERENCES

- [1] J. A. Phillips, D. A. Baker, R. F. Gribble, and C. Munson, "Start-up of Reversed-Field Pinches and Current Ramping Using Dynamo Action," submitted to *Nucl. Fusion* (1987).
- [2] A. A. Newton and P. G. Noonan, "Controlled Termination of Reversed-Field-Pinch Discharges," *Nucl. Instr. and Methods A245* (1986) 167.
- [3] R. L. Hagenson, R. A. Krakowski, C. G. Bathke, R. L. Miller, M. J. Embrechts, N. M. Schnurr, *et al.*, "Compact Reversed-Field Pinch Reactors (CRFPR): Preliminary Engineering Considerations," Los Alamos National Laboratory report LA-10200-MS (August 1984).
- [4] F. Najmabadi, N. M. Ghoniem, R. W. Conn, *et al.*, "The TITAN Reversed-Field-Pinch Fusion Reactor Study: Scoping Phase Report," joint report of UCLA, General Atomics, Los Alamos National Laboratory and Rensselaer Polytechnic Institute, UCLA-PPG-1100 (January 1987).
- [5] P. G. Noonan, C. G. Gimblett, and A. A. Noonan, "Plasma Behavior During Programmed Current Decay and Ramping in the Reversed-Field Pinch," in *Proc. 14th European Conf. on Cont. Fusion and Plasma Phys.*, Madrid, Spain (June 1987).
- [6] A. Kellman, E. Lazzaro, P. Noll, F. C. Schveller, and P. Thomas, "Breakdown Conditions in JET," *Bull. Am. Phys. Soc.* **30** (1985) 1524.
- [7] J. A. Phillips, L. C. Burkhardt, A. Haberstick, R. B. Howell, J. C. Ingraham, E. M. Little, K. S. Thomas, and R. G. Watt, "ZT-40M Current Risetime Study," Los Alamos National Laboratory report LA-9717-MS (1983).
- [8] F. Engelmann, N. Fujisawa, B. B. Kadomtsev, V. I. Pistunovich, J. A. Schmidt, and M. Sugihara, "Physics Design Basis," in *International Tokamak Reactor, Phase One*, IAEA, Vienna (1982) Chap. III, p. 127.
- [9] R. G. Watt and J. N. Downing, "Pre-ionization Studies in ZT-40M," Los Alamos National Laboratory report LA-9163-MS (February 1982).
- [10] J. A. Phillips, Los Alamos National Laboratory, private communication (August 1986).
- [11] H. A. Bodin, R. A. Krakowski, and O. Ortolani, "The Reversed-Field Pinch: from Experiment to Reactor," *Fusion Technol.* **10** (1986) 307.

- [12] G. A. Wurden, P. G. Weber, R. G. Watt, C. P. Munson, T. E. Cayton, and K. Buchl, "Refueling and Density Control in the ZT-40M Reversed-Field Pinch," in *Proc. Int. School of Plasma Phys. Course and Workshop on Physics of Mirrors, Reversed-Field Pinches, and Compact Tori*, Varenna, Italy (September 1987).
- [13] D. B. Thomson (Ed.), *Proc. Int. Workshop on Engineering Design of Next Step Reversed Field Pinch Devices*, Los Alamos National Laboratory (July 13-17, 1987).
- [14] E. W. Larsen, C. D. Levermore, G. C. Pomraning, and J. G. Sanderson, "Discretization Method for One-Dimensional Fokker-Planck Operators," *J. Comp. Phys.* **61** (1985) 359.
- [15] J. S. Chang and G. Cooper, *J. Comp. Phys.* **6** (1970) 1.
- [16] V. D. Shafranov, "Plasma Equilibrium in a Magnetic Field," *Reviews of Plasma Physics* **2**, Consultant Bureau, New York (1966) 103.
- [17] D. A. Baker, L. W. Mann, and K. F. Schoenberg, *Nucl. Fusion* **23** (1983) 380.
- [18] W. A. Press, B. P. Flannery, A. A. Teukolsky, W. A. Vetterling, *Numerical Recipes*, Cambridge University Press, Cambridge, United Kingdom (1986).